PEOPLE'S DEMOCRATIC REPUBLIC OF ALGERIA MINISTRY OF HIGHER EDUCATION AND SCIENTIFIC RESEARCH MOHAMED BOUDIAF UNIVERSITY - M'SILA

FACULTY OF TECHNOLOGY

DEPARTMENT: Electrical engineering

N°:

OPTION: Automatic

SPECIALTY: Automatic and Systems

Title

Machine Learning-Based Predictive Pressure Control in Electrolysis Systems

Presented by:

REGHIOUA MOUSSA

NOUIBAT ALI CHEMSE EDDINE

Defended in front of the jury composed of:

Mr. BOUKHALFA	Abdelouahab	MCA	President
Mr. IDIR	Abdelhakim	Prof	Supervisor
Mr. ZEMMIT	Abderrahim	MCA	Examiner

Academic Year: 2024/2025

Acknowledgments

All praise is due to Allah Almighty, the Most Gracious, the Most Merciful, who granted us the strength, patience, and determination to complete this work. Without His blessings and guidance, none of this would have been possible. We ask Him to accept this humble effort and make it beneficial for us and for all those who seek knowledge.

We want to express our deepest gratitude and sincere appreciation to our esteemed supervisor, **Professor Idir Abdelhakim**, for his unwavering support, invaluable guidance, and insightful feedback throughout the preparation of this thesis. His expertise, constructive criticism, and encouragement were instrumental in shaping the direction of our research and helping us overcome the challenges we faced.

I would also like to express my heartfelt appreciation to Professor **Doghmane Mohmed Zinelabidine** for his generous support and valuable assistance during the completion of this work.

His insightful advice, availability, and encouragement played an important role at critical moments of this project, and for that, I am truly grateful.

We also extend our heartfelt thanks to the respected members of the jury, who honored us with their time, thoughtful reviews, and valuable suggestions that enriched the quality of this work. We are truly grateful for their efforts and dedication.

We extend our sincere appreciation to all the professors and staff members of the **Faculty of Technology, Department of Electrical Engineering at Mohamed Boudiaf University of M'Sila**, for their continuous support, knowledge, and resources provided throughout our academic journey. Their contributions have been vital in equipping us with the skills and foundation necessary for this research.

On a personal note, we owe a profound debt of gratitude to our beloved families, especially our parents, for their unconditional love, patience, sacrifices, and constant encouragement. You have been our backbone and our source of strength, and we dedicate this achievement to you. Your faith in us has always been the guiding light, illuminating us through every difficulty.

To our dear friends and colleagues, thank you for being our companions on this journey; for your moral support, for standing by our side during tough times, for the laughs and motivation, and for sharing both the struggles and the triumphs.

Finally, we would like to extend our appreciation to everyone who, in one way or another, contributed to the completion of this thesis, whether through advice, assistance or simply offering a word of encouragement. Your kindness and support will never be forgotten.

We pray that this work may serve as a small but meaningful contribution to the field and inspire further research and innovation. May Allah bless and reward everyone who has supported us on this journey.

Dedications

To my dear parents, whose love, prayers, and unwavering support have been the foundation of my journey.

To my brothers and sisters, who stood by me with encouragement and strength.

To my beloved family, Reghioua and Doghmane whose presence means everything to me thank you for your inspiration and sense of belonging.

I dedicate this work to all of you, with deep gratitude and love.

Moussa.

To my dear parents, whose love, prayers, and unwavering support have been the foundation of my journey.

To my brothers and sisters, who stood by me with encouragement and strength.

To my beloved family, whose presence means everything to me.

To the kind and proud people of Nouibat and Khaoni—thank you for your inspiration and sense of belonging.

And to my friends, who have shared in my struggles and triumphs with loyalty and joy.

I dedicate this work to all of you, with deep gratitude and love.

Ali chems eddine.

Abstract

This thesis proposes a predictive maintenance model for pressure control systems in electrolysis plants, utilizing advanced machine learning algorithms to enhance the reliability, safety, and efficiency of green hydrogen production. Electrolysis, a cornerstone of green hydrogen production, is often hindered by pressure control component failures, resulting in production losses and safety hazards. Traditional reactive or scheduled maintenance approaches are costly and lead to downtime, further exacerbating inefficiencies. To address these challenges, the proposed framework leverages multivariate operational data and sophisticated machine learning algorithms to proactively predict failures and prevent breakdowns from occurring. Some of the key challenges addressed include the complexities of processing data streams, selecting relevant features, rendering models robust, reducing false alarms, and ensuring simple industrial integration. Moreover, the system incorporates a Proportional-Integral-Derivative (PID) control loop, which is tuned by a Genetic Algorithm for dynamic temperature control of the electrolyzer to maintain optimum operating conditions. The system's efficiency in pressure and temperature stabilization is confirmed by experimental results, resulting in notable operating cost savings, enhanced safety features, and groundbreaking green hydrogen technology. Along with operational improvements, this research lays the groundwork for future studies to optimize maintenance approaches further and enhance the sustainability of hydrogen production. The introduction of machine learning into predictive maintenance not only transforms electrolysis plant operations but also paves the way for the broader adoption of green hydrogen technologies, which are critical to environmental sustainability and energy independence worldwide.

Keywords: *Predictive maintenance; Machine learning algorithms; Electrolysis plants; Green hydrogen production; Pressure control systems; PID control loop.*

ملخص

تُلقي هذه الأطروحة العلمية الضوء على إطار عمل مُتطور للصيانة التنبؤية، قائم بشكل أساسي على تقنيات التعلم الآلي، ومُصمم خصيصًا لأنظمة التحكم في الضغط المُستخدمة في محطات التحليل الكهربائي، ويطمح إلى تعزيز موثوقية وسلامة وكفاءة إنتاج الهيدروجين الأخضر بشكل كبير. لا شك أن الأنظمة المُستخدمة في التحليل الكهربائي تُعدّ محوريةً لتوليد الهيدروجين بشكل مستدام، إلا أن أداءها التشغيلي غالبًا ما يتأثر سلبًا بأعطال في مُكونات التحكم في الضغط، مما قد يُسبب خسائر إنتاجية كبيرة ويُشكل مخاطر أمنية جسيمة. تميل استراتيجيات الصيانة التقليدية، التي تُغلب عليها التفاعلية أو المُجدولة، إلى تكبد تكاليف تشغيلية باهظة، وتؤدي إلى توقفات طويلة، مما يُفاقم من عدم الكفاءة في الإطار التشغيلي. ولمواجهة هذه التحديات، يسعى هذا البحث إلى تطوير نهج صيانة استباقية يُسخّر قوة البيانات التشغيلية مُتعددة المتغيرات، بالتزامن مع خوارزميات التعلم الآلي المُتقدمة، بهدف التنبؤ بالأعطال المُحتملة قبل وقوعها. يتناول النظام المبتكر المقترح هنا العديد من التحديات الحرجة، والتي تشمل على سبيل المثال لا الحصر، تعقيدات تحليل تدفق البيانات، وتحديد أهمية الميزات، وضمان متانة النموذج، وتقليل الإنذارات الكاذبة، وتسهيل التكامل الصناعي السلس. بالإضافة إلى ذلك، تم دمج حلقة تحكم تناسبية-تكاملية-مشتقة (PID)، والتي تم تحسينها بدقة من خلال تطبيق خوارزمية جينية، في الإطار لتنظيم درجة حرارة المحلل الكهربائي ديناميكيًا، مما يضمن ظروف تشغيل مثالية. تُظهر النتائج التجريبية المستمدة من هذا المسعى البحثي بشكل قاطع فعالية الإطار المقترح في الحفاظ على ظروف ضغط ودرجة حرارة مستقرة داخل نظام التحليل الكهربائي، مما يُسهم في نهاية المطاف في خفض كبير في تكاليف التشغيل، وتحسينات في بروتوكولات السلامة، والتقدم التدريجي للتقنيات المرتبطة بإنتاج الهيدروجين الأخضر. علاوة على ذلك، تتجاوز آثار هذا العمل مجرد التحسينات التشغيلية، حيث إنه يُرسي الأساس لجهود بحثية مستقبلية تهدف إلى تحسين ممارسات الصيانة بشكل أكبر وتعزيز الاستدامة الشاملة لعمليات إنتاج الهيدروجين. وفي الختام، فإن دمج التعلم الآلي في الصيانة التنبؤية لا يؤدي إلى إحداث ثورة في النماذج التشغيلية لمحطات التحليل الكهربائي فحسب، بل يعمل أيضًا كمحفز لتبني تقنيات الهيدروجين الأخضر على نطاق أوسع، وهو أمر حاسم لتحقيق الاستدامة البيئية واستقلال الطاقة على نطاق عالمي.

Résumé

Cette thèse propose un modèle de maintenance prédictive pour les systèmes de contrôle de la pression dans les usines d'électrolyse, utilisant des algorithmes d'apprentissage automatique avancés afin d'améliorer la fiabilité, la sécurité et l'efficacité de la production d'hydrogène vert. L'électrolyse, pierre angulaire de la production d'hydrogène vert, est souvent entravée par des défaillances des composants de contrôle de la pression, entraînant des pertes de production et des risques pour la sécurité. Les approches de maintenance traditionnelles, qu'elles soient réactives ou planifiées, s'avèrent coûteuses et provoquent des arrêts prolongés, aggravant ainsi les inefficacités opérationnelles. Pour relever ces défis, le cadre proposé exploite des données opérationnelles multivariées et des algorithmes d'apprentissage automatique sophistiqués afin de prédire de manière proactive les pannes et d'empêcher leur survenue. Parmi les principaux défis abordés figurent la complexité du traitement des flux de données, la sélection des caractéristiques pertinentes, le renforcement de la robustesse des modèles, la réduction des fausses alertes, et l'assurance d'une intégration industrielle simple. De plus, le système intègre une boucle de contrôle proportionnelle-intégrale-dérivée (PID), réglée par un algorithme génétique pour un contrôle dynamique de la température de l'électrolyseur, assurant ainsi des conditions de fonctionnement optimales. Les résultats expérimentaux confirment l'efficacité du système dans la stabilisation de la pression et de la température, se traduisant par des économies de coûts d'exploitation significatives, une amélioration des dispositifs de sécurité, et des avancées majeures dans la technologie de l'hydrogène vert. En plus des améliorations opérationnelles, cette recherche jette les bases d'études futures visant à optimiser davantage les stratégies de maintenance et à renforcer la durabilité de la production d'hydrogène. L'introduction de l'apprentissage automatique dans la maintenance prédictive transforme non seulement le fonctionnement des usines d'électrolyse, mais ouvre également la voie à une adoption plus large des technologies de l'hydrogène vert, essentielles à la durabilité environnementale et à l'indépendance énergétique mondiale.

Mots-clés : Maintenance prédictive ; Algorithmes d'apprentissage automatique ; Usines d'électrolyse ; Production d'hydrogène vert ; Systèmes de contrôle de la pression ; Boucle de contrôle PID.

List of Symbols

Symbol	Description	Unit
V	Voltage	Volts (V)
I	Current	Amperes (A)
R	Resistance	Ohms (Ω)
C	Capacitance	Farads (F)
L	Inductance	Henrys (H)
P	Power	Watts (W)
f	Frequency	Hertz (Hz)
ω	Angular frequency	rad/s
τ	Time constant	s
T	Temperature / Sampling period	°C / s
T_el	Electrolyzer temperature	°C
T_bt_out	Buffer tank outlet temperature	°C
T_El_in	Electrolyzer inlet temperature	°C
T_cw_out	Cooling water outlet temperature	°C
T_setpoint	Temperature setpoint	°C
s	Laplace transform variable	-
G(s)	Transfer function	-
u(t)	Input signal	-
y(t)	Output signal	-
e(t)	Error signal	-
Kp, Ki, Kd	PID controller gains	-
J	Moment of inertia	kg·m²
θ, θ̇	Angular position / velocity	rad / rad/s
Δ	Change / Variation	-
F, F_const	Faraday constant	96485 C/mol
R (gas)	Universal gas constant	J/mol·K
Utn	Thermoneutral voltage	Volts (V)
Cp, Cp_lye	Specific heat capacity of water/lye	J/g·K
A, A_el	Electrode area	m²
q_cw	Cooling water flow rate	g/s
N	Number of electrolyzers	-
nc	Number of cells per electrolyzer	-
Pnet	Total input power	Watts (W)
x(t)	State vector	various
dx/dt	Time derivative of states	varies
Psto_H2, Psto_O2	Storage pressure of H_2 / O_2	bar
Mass_Bt	Buffer tank mass	kg or g
Q_generated	Generated heat	J or W
Q_loss	Heat loss	J or W
Q_net	Net heat	J or W
Water_consumption	Electrolysis water consumption	g/s
α, k, σ	Efficiency / conductivity / Stefan-Boltzmann	various
Vc, Vh	Cold/hot side volumes in heat exchanger	m³
T_ref	Reference temperature	K

List of Figures

List of Tables

Table of Content

Problematic

The demand for green hydrogen production has increased, so unexpected failures in the pressure control systems of electrolysis plants will drastically cut production and create a serious safety hazard. Maintenance in such facilities is predominantly scheduled, along with corrective actions performed after failure scenarios that can lead to several issues, including unnecessary downtime, increased operational costs, and potential safety hazards. Although various sensors and monitoring systems are already available, the complex interactions between components and operating conditions make the precise prediction or avoidance of these pressure control system failures quite challenging. This issue creates an urgent demand for sophisticated maintenance methods that can utilize vast quantities of operational data to predict possible failures before they happen. While incorporating machine learning techniques is promising, several challenges must be addressed, such as how to effectively process and analyze multivariate data streams from pressure control systems to identify subtle patterns that indicate imminent failures. What is the relevance of parameters and features in making more accurate failure predictions? How can we develop robust models that minimize false alarms while ensuring that no critical failures are overlooked? Besides, introducing such systems raises questions about finding an optimal balance between maintenance costs and the system's reliability, as well as the practical integration aspects of the predictive maintenance system into the current industrial environment. This thesis will develop and validate a comprehensive ML-based predictive maintenance framework specifically tailored for pressure control systems in electrolysis plants.

Key Questions:

How can unexpected failures in pressure control systems of electrolysis plants be predicted and prevented to ensure continuous green hydrogen production and operational safety?

How should relevant parameters and features be selected and prioritized to improve the accuracy of failure predictions in pressure control systems?

How can predictive maintenance contribute to the long-term sustainability and scalability of green hydrogen production technologies?

Chapter 1: Introduction

Water electrolysis was first performed by *Jan Rudolph Deiman* and *Adriaan Paets van Troostwijk* in 1789 [1], using electricity produced by an electrostatic machine and discharged on gold electrodes in water. In 1800, *Alessandro Volta* applied his voltaic pile to water electrolysis, but the results were not widely studied. The same year, *W. Nicholson and A. Carlisle* conducted water electrolysis experiments using copper electrodes and a voltaic pile. *J. Ritter* performed absolute water electrolysis, collecting oxygen and hydrogen gases separately [2]. However, industrial application of water electrolysis only began at the end of the nineteenth century, with over 400 electrolysis units in operation by 1902. Technical and engineering reasons for this delay included the time required to develop suitable DC power sources and efficient diaphragms to separate anode and cathode chambers [3].

Hydrogen is essential for various industrial applications, including the production of ammonia, methanol, petroleum products, and polymers. Currently, most hydrogen is produced through the steam reforming of fossil hydrocarbons, which causes pollution (Fig. 1.1).

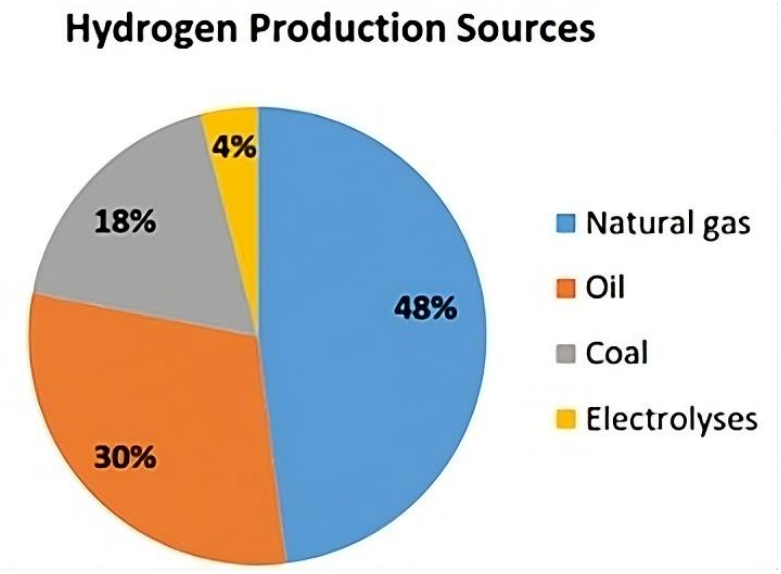

Figure 1.1: Hydrogen production sources [14].

Water electrolysis is essential for hydrogen production and for distributed on-demand and on-site generation solutions, creating a carbon-free and environmentally friendly economy. This solution will help reduce atmospheric CO2 emissions and promote a more sustainable future [4, 5].

Electrolysis is a promising method for carbon-free hydrogen production from renewable and nuclear resources. It involves splitting water into hydrogen and oxygen using electricity. It is performed in an electrolyzed form (Fig. 1.2). Electrolyzers range from tiny appliances for distributed hydrogen production to extensive, central facilities connected to renewable or non-greenhouse gas-emitting electricity sources.

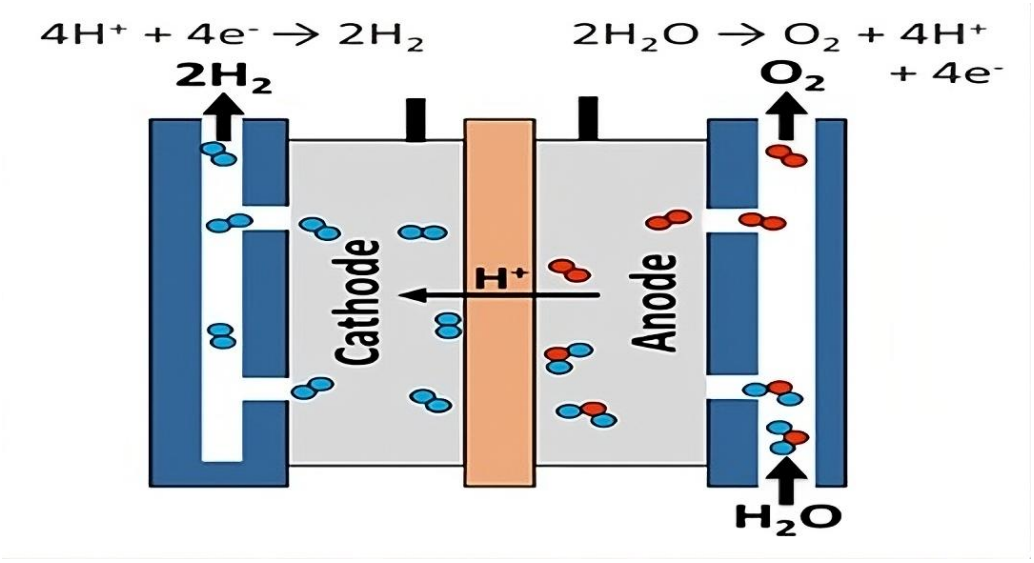

Figure 1.2: Principle of generation of H2 from H2O in Electrolysis

Hydrogen production via electrolysis could synergize with dynamic and intermittent power generation in renewable energy technologies. Wind power variability can hinder its practical use, but integrating hydrogen fuel and electric power generation at wind farms can provide flexibility in resource allocation (Fig.1.3). Additionally, excess electricity from wind farms can produce hydrogen through electrolysis instead of curtailing it, allowing for better resource utilization and market factors [6].

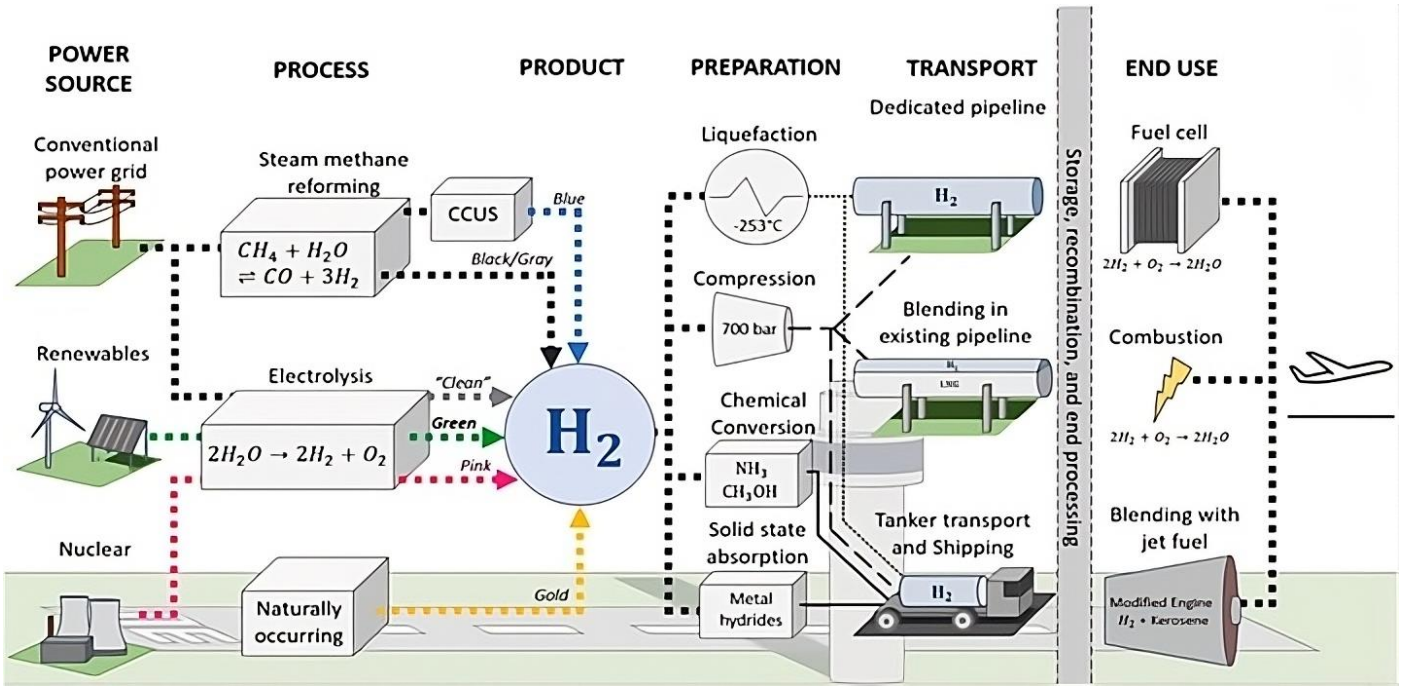

Figure 1.3: Diagrammatic illustration of the sources and applications of hydrogen for use in aviation

1. Context and Industrial Challenges

In recent years, extreme weather events have led to a push to limit global warming to within 2°C by the end of the 21st century. Countries are making significant efforts to transition their energy systems from fossil fuels towards low-carbon or carbon-free energy production. The structure of global production and consumption of traditional fossil fuels and renewable energy resources will be reshaped as countries recognize the importance of energy security and focus on energy production and consumption.

Hydrogen energy is a renewable, clean, and efficient secondary energy source with numerous advantages, including abundant sources, a high calorific value of combustion, clean and pollution-free usage, diverse utilization forms, a potential energy storage medium, and safety. As the world faces increasing pressure from climate change and natural disasters, hydrogen energy has become a strategic choice for many countries' energy transformation.

According to the Global Hydrogen Review 2021 and China's Medium and Long-Term Plan for the Development of the Hydrogen Industry (2021–2035), global annual hydrogen production is approximately $9{,}000 \times 10^4$ t, with China's annual production being $3{,}300 \times 10^4$ t. In 2021, 142 new hydrogen stations were opened globally, bringing the total number of stations to 685 worldwide. Asia has the highest number of hydrogen refueling stations (363), mainly in China, Japan, and South Korea.

Over 20 countries or alliances have released or formulated national hydrogen energy strategies. The United States has long promoted hydrogen's unique position and advantages in the future energy system. At the same time, the European Union supports the development of hydrogen energy and fuel cells. Japan's government proposed a strategy of "building a hydrogen-based society ahead of other countries" in 2017. China incorporated hydrogen into its 14th Five-Year Plan and the 2035 Vision 2020 to achieve the strategic goals of "peaking CO2 emissions and carbon neutrality." [7].

2. Role of pressure control in electrolysis

Pressure management is crucial in electrolysis, particularly in industrial applications such as water electrolysis, hydrogen generation, and chlor-alkali processes. Why it matters is as follows:

- **Separation and Purity of Gas**

  The cathode and anode of water electrolysis produce hydrogen and oxygen gases, respectively. Maintaining the pressure at the proper level helps prevent contamination and gas leakage. Because differential pressure management prevents the gases from mixing, it increases purity and reduces the likelihood of an explosion.

- **Efficiency as well as Energy Use**
    1. The energy required for compression in later phases of storage or transportation can be reduced by increasing the pressure.
    2. Excessive pressure raises the electrolyte's electrical resistance and may decrease efficiency.
    3. These variables are balanced to optimize pressure management, resulting in reduced energy usage.

- **Control of Electrolytes**
    1. Under proper pressure, the electrolyte cannot evaporate too rapidly or generate undesirable bubbles, which might damage the electrode surface and decrease efficiency.
    2. Pressure maintains a steady electrolyte flow during high-pressure electrolysis, such as PEM electrolysis.

- **Safety and Structural Soundness**
    1. Electrolysis cells and their constituent parts must be able to tolerate changes in internal pressure to prevent leaks or malfunctions.
    2. Underpressure can result in unintended side effects or gas backflow, while overpressure can harm cells.

- **Rate of Reaction and Solubility in Gas**
    1. Pressure affects the soluble gasses in the electrolyte. At higher pressures, more gas dissolving in the liquid may slow down gas evolution or cause problems with bubble formation.
    2. A constant response rate and avoidance of efficiency losses are guaranteed by controlled pressure. [8, 9, 10 11, 12].

3. Potential of ML in maintenance

Machine learning has revolutionized Industry 4.0 by enabling companies to adopt proactive strategies for predictive maintenance. This approach not only increases efficiency and reduces downtime but also optimizes resource utilization. As businesses explore sustainable technology, the traditional "break-fix" model is no longer sufficient. As ML algorithms advance, businesses can use data for more intelligent decision-making, predicting equipment failures before they occur. This prediction enables targeted maintenance, reduces emergency repairs, lowers energy consumption, and fosters a more sustainable operational framework. This article examines the application of machine learning in predictive maintenance and how organizations can utilize these solutions.

Machine learning (ML) is transforming the maintenance industry by analyzing vast amounts of data from sensors and historical records to identify potential equipment failures. ML algorithms learn from this data to recognize abnormalities and predict when maintenance will likely be required. For example, in solar power facilities, panel sensors collect data on various parameters, enabling the prediction of potential issues such as deteriorating panel efficiency or faulty components. By proactively scheduling maintenance based on these predictions, facilities can ensure optimal energy production and enhance the efficiency of renewable energy generation.

The global predictive maintenance market is projected to reach $31,965.49 million by 2027, growing at a compound annual growth rate (CAGR) of 28.8% from 2020 to 2027. According to a McKinsey survey, 84% of respondents already adopt predictive maintenance approaches for critical assets. In mature reliability-centered maintenance (RCM) capabilities, 70-85% of technician hours are spent on preventative maintenance (PM) activities.

Traditional maintenance was reactive, relying on fixed equipment and predefined schedules, which often led to over-maintenance or missed opportunities for timely intervention. ML-driven maintenance introduces a more dynamic and adaptive model, enabling precisely timed maintenance through continuous data analysis. This approach can reduce costs, reduce downtime, and increase the efficiency of renewable energy generation.

3.1 Traditional vs ML Maintenance

Traditionally, maintenance was reactive, focusing on addressing fixed issues and adhering to predefined schedules. This approach led to over-maintenance, missed opportunities, increased costs, and a less-than-ideal environmental footprint. Machine learning has introduced a more dynamic model, enabling precise, timely maintenance by continuously analyzing data. This comparison highlights the benefits of ML-driven maintenance over traditional methods. Table 1 summarizes the primary differences between traditional and machine learning (ML)-driven predictive maintenance methods.

Table 1: Comparison between traditional maintenance methods vs. ML-driven predictive maintenance

Traditional maintenance	ML-driven predictive maintenance
Reactive approach	Proactive intervention
Fixed maintenance schedule	Dynamic and adaptive maintenance
Routine checks	Real-time health monitoring
Limited data handling	Analysis of large datasets
Unplanned downtime	Predictions of failures in advance
Increased costs	Optimized operational efficiency

3.2 The Future of Predictive Maintenance with ML

The future of predictive maintenance, driven by machine learning (ML), is expected to see significant advancements. Edge computing, which utilizes data closer to the source, is crucial for real-time decision-making, enabling immediate responses to potential issues and minimizing downtime. Digital twins, which are still in their early stages, will enable more accurate simulations and predictive modeling, thereby improving maintenance strategies and enhancing understanding of asset behavior throughout their lifespan. Explainable AI, dedicated to making machine learning models more interpretable, is essential for transparency in decision-making, ensuring that recommendations and insights provided by ML algorithms are clear and easy to check. This trust and effective collaboration between humans and AI facilitate more informed decisions.

Autonomous maintenance robots are expected to integrate into the industrial landscape, conducting routine inspections, identifying potential issues, and performing minor repairs. This shift towards autonomous maintenance aims to reduce human exposure to hazardous environments and partially solve the human talent shortage. As reliance on AI and ML algorithms grows, the future of predictive maintenance will likely see a shift towards these advancements.

3.3 The Strategic Advantage of ML in Predictive Maintenance

Machine learning (ML) provides a strategic advantage in predictive maintenance, enabling businesses to plan maintenance activities more effectively, thereby reducing downtime and costs. This approach is crucial in the era of Industry 4.0, where modern maintenance strategies are interconnected and can evolve from reactive to proactive and predictive models [13]. Fig. 1.4 summarizes the benefits of using machine learning (ML) for predictive models in the industry.

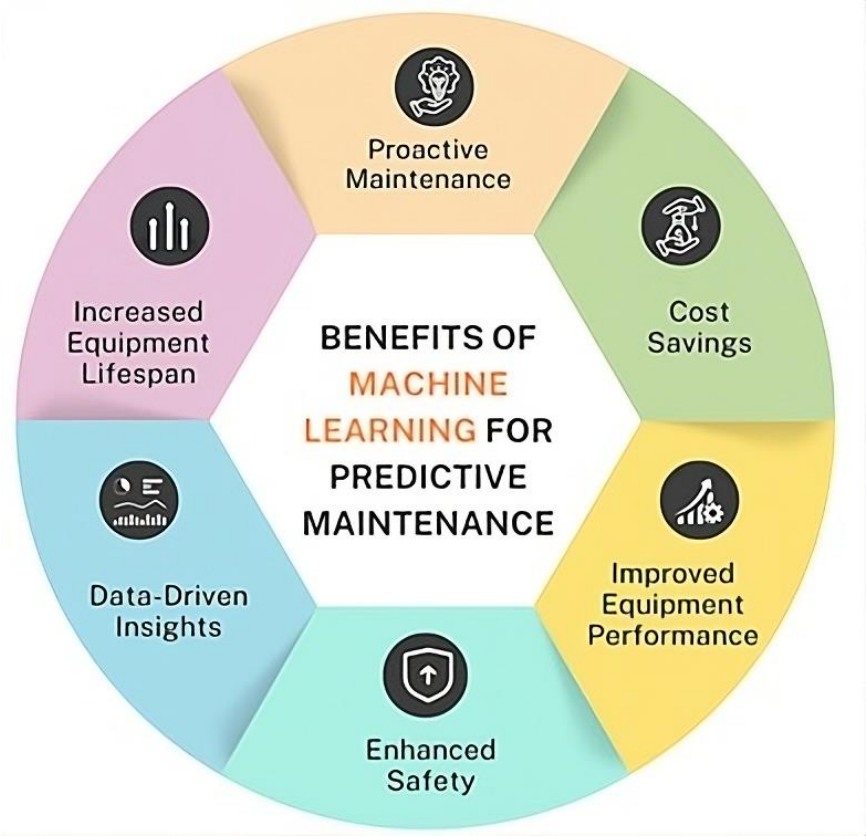

Figure 1.4: Benefits of using ML for predictive models in the industry in general.

4. Research Objectives

The main objectives of our master thesis are:

1. **Develop a Machine Learning-Based Predictive Maintenance Framework:** In this step, we will design and implement a complete system tailored to pressure control in electrolysis plants, capable of predicting failures before they occur.

2. **Analyze Multivariate Data Streams:** This sub-objective involves processing and analyzing complex, high-dimensional sensor data to detect subtle patterns and early warning signs of pressure anomalies.

3. **Feature Relevance and Model Optimization:** We will investigate the most critical parameters and features for accurate failure predictions, balancing model accuracy with interpretability.

4. **Minimize False Alarms and Maximize Reliability:** Build robust ML models that reduce false positives while ensuring no critical failures go unnoticed.

5. **Optimize Maintenance Scheduling:** Based on predictive insights, the transition from scheduled maintenance to condition-based and predictive maintenance strategies.

6. **Facilitate Industrial Integration:** We will address practical integration challenges, ensuring the predictive system seamlessly fits within existing industrial infrastructure and workflows.

7. **Balance Cost and System Reliability:** By exploring the trade-off between maintenance costs and system reliability, we aim to strike the optimal balance for sustainable plant operations. This enables us to overcome the primary drawback of blue hydrogen generated through electrolysis, which is its high cost.

4. Conclusion

In this chapter, we present an overview of water electrolysis as a flagship technology for green hydrogen production, tracing its historical roots and industrial applications. It reflects the growing global demand for energy sourced from hydrogen, driven by a desire to transition away from fossil fuels and towards low-carbon energy sources. The chapter addresses industrial concerns, including energy efficiency, safety, and the role of pressure control systems in maintaining gas purity, optimizing energy utilization, and ensuring system integrity. It also introduces the potential of machine learning (ML) in predictive maintenance, where it outshines traditional maintenance techniques. ML allows for real-time monitoring, early failure prediction, and optimal maintenance scheduling, reducing downtime and operating costs. The chapter concludes with the research goals, which involve developing an ML-based predictive maintenance framework for pressure control systems in electrolysis plants. This framework addresses key challenges, including feature selection, model reliability, and integration into the industry, to enhance efficiency and sustainability.

The next chapter will outline the state-of-the-art machine learning approaches in predictive maintenance for electrolysis systems. This literature review will discuss existing methodologies, examine their merits and limitations, and identify the most suitable machine learning (ML) methods for predicting failure in pressure control systems. These developments will provide a solid foundation for designing an optimal predictive maintenance strategy that ensures the maximum reliability and sustainability of green hydrogen production.

References

[1]. Pasquale Cavaliere, Water Electrolysis for Hydrogen Production, Springer Book, DOI: https://doi.org/10.1007/978-3-031-37780-8

[2]. Faisal S. AlHumaidan, Mamun Absi Halabi, Mohan S. Rana, Mari Vinoba, Blue hydrogen: Current status and future technologies, Energy Conversion and Management, Volume 283, 2023, https://doi.org/10.1016/j.enconman.2023.116840

[3]. Sixie Zhang, Wenwen Xu, Haocheng Chen, Qihao Yang, et al., Progress in Anode Stability Improvement for Seawater Electrolysis to Produce Hydrogen, Review paper, Advanced Materials, Volume36, Issue37 Special Issue: Two Decades of Materials Research Excellence at Ningbo Institute of Materials Technology and Engineering (NIMTE, CAS), September 12, 2024

[4]. Wonjun Noh, Inkyu Lee, Synergizing autothermal reforming hydrogen production and carbon dioxide electrolysis: Enhancing the competitiveness of blue hydrogen in sustainable energy systems, Chemical Engineering Journal, Volume 499, 2024, https://doi.org/10.1016/j.cej.2024.156688

[5]. Seunggwan Yun, Jaewon Lee, Hyungtae Cho, Junghwan Kim, Oxy-fuel combustion-based blue hydrogen production with the integration of water electrolysis, Energy Conversion and Management, Volume 291, 2023, https://doi.org/10.1016/j.enconman.2023.117275

[6]. A. Ajanovic, M. Sayer, R. Haas, The economics and the environmental benignity of different colors of hydrogen, International Journal of Hydrogen Energy, Volume 47, Issue 57, 2022, Pages 24136-24154, https://doi.org/10.1016/j.ijhydene.2022.02.094

[7]. Jan Frederick George, Viktor Paul Müller, Jenny Winkler, Mario Ragwitz, Is blue hydrogen a bridging technology? - The limits of a CO2 price and the role of state-induced price components for green hydrogen production in Germany, Energy Policy, Volume 167, 2022, 113072, https://doi.org/10.1016/j.enpol.2022.113072

[8]. Andrzej Lasia, Mechanism and kinetics of the hydrogen evolution reaction, International Journal of Hydrogen Energy, Volume 44, Issue 36, 2019, Pages 19484-19518, https://doi.org/10.1016/j.ijhydene.2019.05.183

[9]. Youssef Naimi and amal antar, Hydrogen Generation by water electrolysis, book chapter 1, Advances In Hydrogen Generation Technologies, http://dx.doi.org/10.5772/intechopen.76814

[10]. Houcheng Zhang, Guoxing Lin, Jincan Chen, Evaluation and calculation on the efficiency of a water electrolysis system for hydrogen production, International Journal of Hydrogen Energy, Volume 35, Issue 20, 2010, Pages 10851-10858, https://doi.org/10.1016/j.ijhydene.2010.07.088

[11]. Mingyong Wang, Zhi Wang, Xuzhong Gong, Zhancheng Guo, The intensification technologies to water electrolysis for hydrogen production – A review, Renewable and Sustainable Energy Reviews, Volume 29, 2014, Pages 573-588, https://doi.org/10.1016/j.rser.2013.08.090

[12]. A. Ursua, L. M. Gandia and P. Sanchis, "Hydrogen Production From Water Electrolysis: Current Status and Future Trends," in *Proceedings of the IEEE*, vol. 100, no. 2, pp. 410-426, Feb. 2012, doi: 10.1109/JPROC.2011.2156750

[13]. Álvaro Serna, Imene Yahyaoui, Julio E. Normey-Rico, César de Prada, Fernando Tadeo, Predictive control for hydrogen production by electrolysis in an offshore platform using renewable energies, International Journal of Hydrogen Energy, Volume 42, Issue 17, 2017, Pages 12865-12876, https://doi.org/10.1016/j.ijhydene.2016.11.077

[14]. Meryem Gizem Sürer and Hüseyin Turan Arat, State of art of hydrogen usage as a fuel on aviation, European Mechanical Science 2018, Vol. 2(1): 20-30, DOI: 10.26701/ems.364286

Chapter 2

II. Literature Review

2.1 Electrolysis pressure control systems:

The regulation and management of pressure within electrolyzes represent an exceptionally critical and essential aspect of ensuring optimal system efficiency, safety, and overall performance across a myriad of diverse industrial applications, which prominently include, but are not limited to, hydrogen production and water treatment processes. Previous scholarly research has emphasized the importance of maintaining precise pressure control, as any imbalances that may occur can lead to detrimental operational inefficiencies or even catastrophic equipment failures, underscoring the need for rigorous pressure management protocols.

2.1.1 Key Components of Pressure Control Systems

An extensive body of studies has identified several core components that are essential for effective pressure management in electrolysis systems, each of which plays a pivotal role in the overall functionality of these systems:

- **Pressure Sensors**: These sophisticated devices are specifically designed to accurately measure the pressure of the gases generated during the electrolysis process. They provide critical real-time data that enables necessary system adjustments to be made swiftly (*Chi-Yuan et al., 2024*) in [1].

- **Control Valves**: Research in this area indicates that control valves are crucial components that play a vital role in adjusting the flow of gases to maintain the desired pressure levels within the system, thereby ensuring operational stability (*AlZahrani & Dincer, 2018*) in [2].

- **PID Controllers**: According to recent advancements in control technology, PID controllers automatically regulate pressure by fine-tuning the positions of valves in direct response to feedback received from sensors, which significantly improves the system's overall stability and reliability (*Lixia et al., 2025*) [3].

- **Backpressure Regulators**: These important components maintain a predetermined set pressure by effectively releasing any excess gas that may be generated, thereby mitigating the risk of over-pressurization, which could lead to dangerous operational conditions (*Bazarah et al., 2022*) [4].

- **Safety Relief Valves**: Numerous safety studies have emphasized the critical importance of relief valves in preventing hazardous overpressure conditions, which can pose significant risks to equipment integrity and personnel safety (*Scuro et al, 2018*) [5].

- **Flow Meters**: Flow meters play a crucial role in ensuring a balanced output of gases, which is essential for synchronizing the production rates of hydrogen and oxygen, thereby optimizing the overall efficiency of the electrolysis process (*Ito et al, 2010*) [6].

- **Electrolyzer Stack Design**: The literature suggests that the design of the electrolyzer stack has a pronounced influence on pressure balance, with specific cell configurations directly impacting the overall stability and performance of the system (*Rizwan et al., 2021*) [7].

2.1.2 Working Principles and System Dynamics

The electrolysis process itself inherently involves the splitting of water molecules into hydrogen and oxygen gases through the application of an electric current. As the produced gases accumulate in their respective chambers, it becomes imperative to maintain meticulous pressure balancing to prevent potential damage to the electrolyzer membranes or hazardous leaks. Research in this field highlights the effectiveness of feedback loops, wherein sensors and controllers continuously adjust gas flow and valve settings to maintain stable pressure levels, thereby ensuring a safe and efficient electrolysis process (*Selamet at al., 2011*) [8].

2.2 Common failure modes and mechanisms

Failures in engineering systems are extensively analyzed and scrutinized within the engineering field due to their profound ramifications on safety protocols, reliability assessments, and the overall economic performance of various systems. Exploring different failure modes is crucial, as these failures can arise from various factors, including diverse loading conditions, environmental influences, and the inherent properties of the materials themselves. This literature review presents a comprehensive examination of prevalent failure modes, their underlying mechanisms, and pertinent references that aim to enhance understanding of these critical engineering issues.

Fatigue failure is a phenomenon that occurs as a direct consequence of repeated cyclic loading, ultimately leading to the initiation and subsequent propagation of cracks within the material. Numerous studies have indicated that microcracks frequently originate at points of stress concentration, such as notches or surface imperfections, and these cracks tend to propagate under conditions of fluctuating stress, as elucidated by *Kuhnert in 2023*. It is important to note that fatigue failures are commonly observed across various sectors,

including aerospace, automotive, and structural applications, particularly in scenarios where cyclic loading is a predominant operational characteristic [9].

Corrosion failure represents a significant challenge in engineering systems, as it involves the degradation of materials due to various chemical reactions within their environment. Corrosion can manifest in several distinct forms, including uniform corrosion, which involves the gradual thinning of material due to consistent exposure to corrosive environments; pitting corrosion, which results in the formation of localized deep holes that can severely compromise structural integrity; and stress corrosion cracking (SCC), which arises under the synergistic effects of tensile stress in conjunction with corrosive media, as discussed by *Prestat in 2023*. The implications of corrosion failures are particularly critical in marine, chemical processing, and infrastructure industries, where materials are continually subjected to harsh and aggressive environmental conditions [10].

Creep failure is characterized by time-dependent deformation that occurs when materials are subjected to a constant load, particularly at elevated temperatures. Research conducted in the field suggests that creep results from atomic diffusion and the sliding of grain boundaries, which collectively lead to the elongation of materials followed by eventual rupture, as noted by *Arthurs and Kusoglu in 2021*. This particular failure mode is commonly encountered in applications involving turbines, boilers, and aerospace components operating under high temperatures [11].

Wear failure signifies material degradation due to mechanical interactions between contacting surfaces, leading to surface deterioration over time. The mechanisms of wear can be classified into several categories, including adhesive wear, in which material is transferred between surfaces due to intense adhesive forces; abrasive wear, which is instigated by hard particles that scratch the material; and fretting wear, which arises from oscillatory micro-motions, a concept explored by *Bairamov in 2020*. The impact of wear failures is particularly pronounced in components such as bearings, gears, and various machine elements integral to the manufacturing and transportation industries [12].

Brittle fracture is a failure mode characterized by a sudden and catastrophic failure with minimal plastic deformation evident in the material. This failure mode typically occurs due to rapid crack propagation in materials that exhibit low toughness, which is often influenced by factors such as temperature and inherent material defects, as originally described by *Aldakhil et al. (2022)*. The prevalence of brittle fractures is particularly notable in materials such as ceramics and high-strength steels, as well as in environments characterized by low temperatures [13].

In contrast to the brittle fracture, ductile failure is a mode of failure characterized by gradual deformation prior to the material's ultimate rupture. This process is predominantly governed by microvoid coalescence, which leads to necking and eventual fracture, as discussed. Ductile failure is commonly observed in metals and alloys

subjected to excessive tensile loads, and understanding this mechanism is crucial for material selection and structural design [8].

Buckling failure occurs when a structure loses stability under compressive loads, resulting in either elastic or plastic instability that leads to significant lateral deformations. Such deformations can ultimately lead to catastrophic structural collapse, as highlighted in the work of *Kink et al. (2024*). The buckling phenomenon is particularly concerning in slender structural elements, such as columns and beams, and in aerospace structures, where stability is paramount [14].

Thermal fatigue failure is a specific type that arises due to cyclic thermal stresses, which induce crack formation at points of stress concentration within materials. The repeated expansion and contraction of materials subjected to fluctuating temperature conditions can induce localized damage that ultimately leads to failure, a phenomenon thoroughly investigated by *Zachary et al. (2023*). This type of failure is commonly observed in engine components, exhaust systems, and high-temperature piping, where thermal cycling is an integral aspect of operational performance [15].

2.3 Traditional maintenance approaches

Traditional maintenance approaches focus on routine and reactive methods to keep equipment and systems running (Fig. 2.1). Here are some key types with references:

1. **Reactive Maintenance (Run-to-Failure)**
    - ✓ Equipment is repaired only after a failure occurs.
    - ✓ Pros: Low initial cost, simple implementation.
    - ✓ Cons: High downtime and unpredictable costs.
2. **Preventive Maintenance (Time-Based Maintenance)**
    - ✓ Scheduled maintenance at regular intervals to prevent failures.
    - ✓ Pros: Reduces unexpected breakdowns and extends equipment life.
    - ✓ Cons: This can lead to unnecessary maintenance and higher labor costs.
3. **Corrective Maintenance**
    - ✓ Fixing small issues before they turn into major failures.
    - ✓ Pros: It increases reliability and is less costly than reactive maintenance.
    - ✓ Cons: It requires monitoring and may not prevent all failures.
4. **Condition-Based Maintenance (CBM)**
    - ✓ Maintenance is performed based on real-time condition monitoring.
    - ✓ Pros: Reduces unnecessary maintenance and improves efficiency.
    - ✓ Cons: It requires advanced monitoring systems and a higher initial investment.

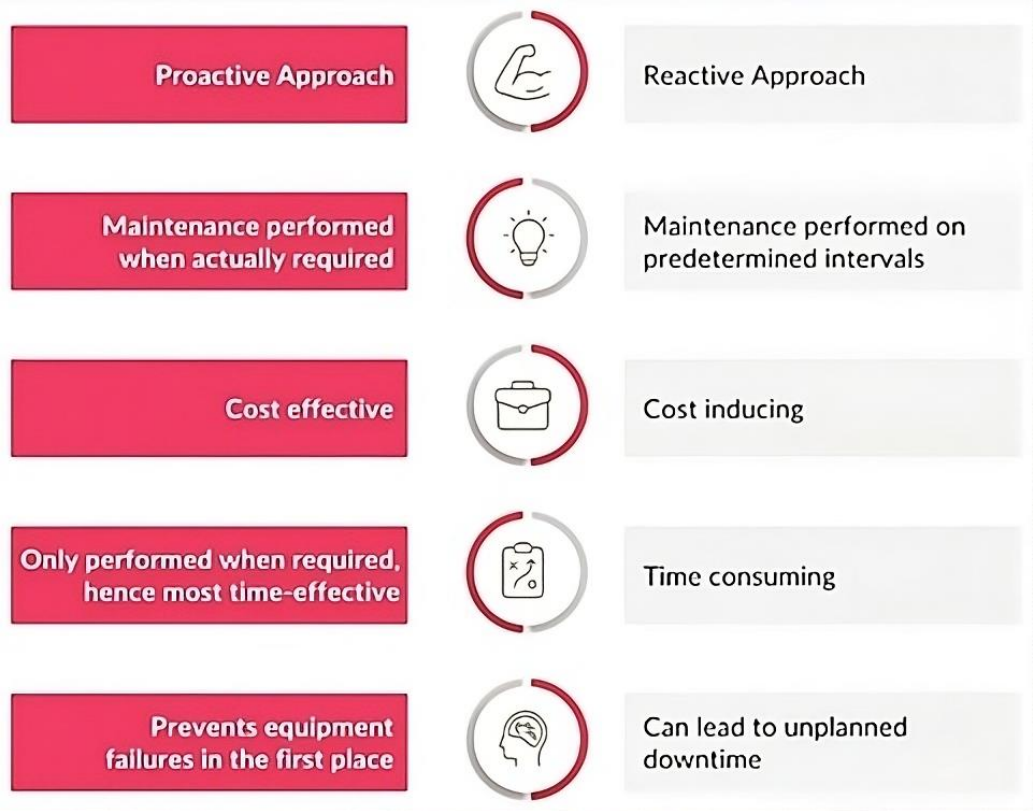

Figure 2.1: Predictive Maintenance vs Traditional Maintenance

2.4 ML applications in industrial maintenance

Machine learning (ML), which refers to the development of algorithms that enable computers to learn from and make predictions based on data, has undeniably emerged as a revolutionary force in industrial maintenance. It significantly assists organizations in optimizing their operational processes, reducing instances of unplanned downtime, and ultimately achieving substantial cost savings. To fully comprehend the transformative impact of this technology, let us delve into a detailed examination of its key applications within the realm of industrial maintenance.

2.4.1 Key Applications of Machine Learning in the Field of Industrial Maintenance

1. Predictive Maintenance

The deployment of machine learning models is crucial in analyzing sensor-generated data, which includes vibrations, temperature variations, and pressure measurements. This enables the identification of specific patterns that can accurately predict equipment failures before they occur. This advanced predictive capability enables the scheduling of maintenance activities only, when necessary, significantly reducing the likelihood of unplanned downtime and concurrently minimizing the associated costs of maintenance operations [15].

2. Anomaly Detection:

Machine learning technologies employ sophisticated algorithms to identify outliers within operational data, which serve as indicators of abnormal behavior or potential malfunctions in the equipment. The provision of real-time alerts empowers operators to take prompt corrective actions in response to these anomalies, thereby mitigating the risk of operational disruptions and enhancing overall system reliability.

3. Condition Monitoring:

The continuous monitoring of machine health is achieved by integrating Internet of Things (IoT) sensors with machine learning models, providing a comprehensive overview of equipment performance. This ongoing assessment enables the meticulous tracking of wear and tear and the prediction of component degradation over an extended period, allowing for preemptive measures to be taken before significant issues arise [16].

4. Failure Root Cause Analysis:

By leveraging historical failure data, machine learning techniques can analyze the information to identify the fundamental causes of recurring issues plaguing machinery. This analytical process not only aids engineers in implementing targeted improvements but also facilitates the redesign of faulty components, thereby enhancing the overall durability and reliability of the equipment.

5. Inventory Optimization:

Machine learning algorithms are used to forecast the demand for spare parts with remarkable accuracy, based on predictions related to equipment failures, thereby preventing overstocking and shortages of critical components. As a result, organizations can significantly reduce inventory carrying costs while ensuring that essential parts remain readily available when required, streamlining maintenance operations.

6. Digital Twins:

The concept of digital twins involves creating virtual replicas of physical systems powered by machine learning technologies. These digital representations enable the simulation of various scenarios, allowing for the prediction of machine behavior under diverse conditions. This, in turn, helps optimize overall equipment performance and operational efficiency.

7. Work Order Prioritization:

Machine learning algorithms play a pivotal role in prioritizing maintenance work orders by assessing the severity and potential impact of each task on production activities. This systematic ranking process empowers

maintenance teams to concentrate on addressing the most critical issues first, thereby significantly improving operational efficiency and minimizing disruptions to production workflows.

2.5 Data acquisition and sensor technologies

2.5.1 What is a Data Acquisition System?

A data acquisition system is a combination of sensors, measurement devices, and a computer used to gather and process data to analyze electrical or physical phenomena, providing a comprehensive understanding (Fig. 2.2).

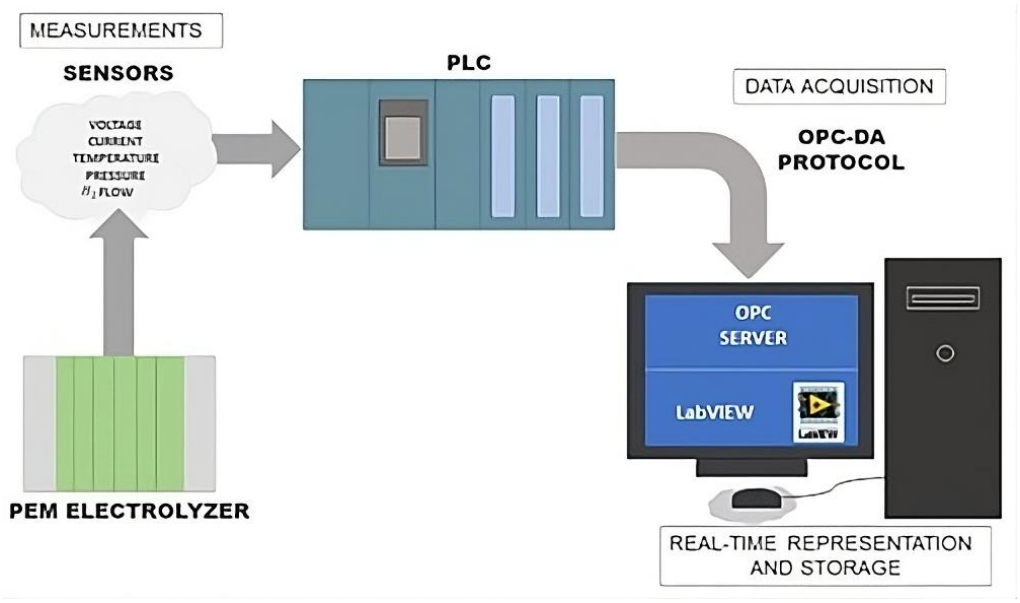

(a)

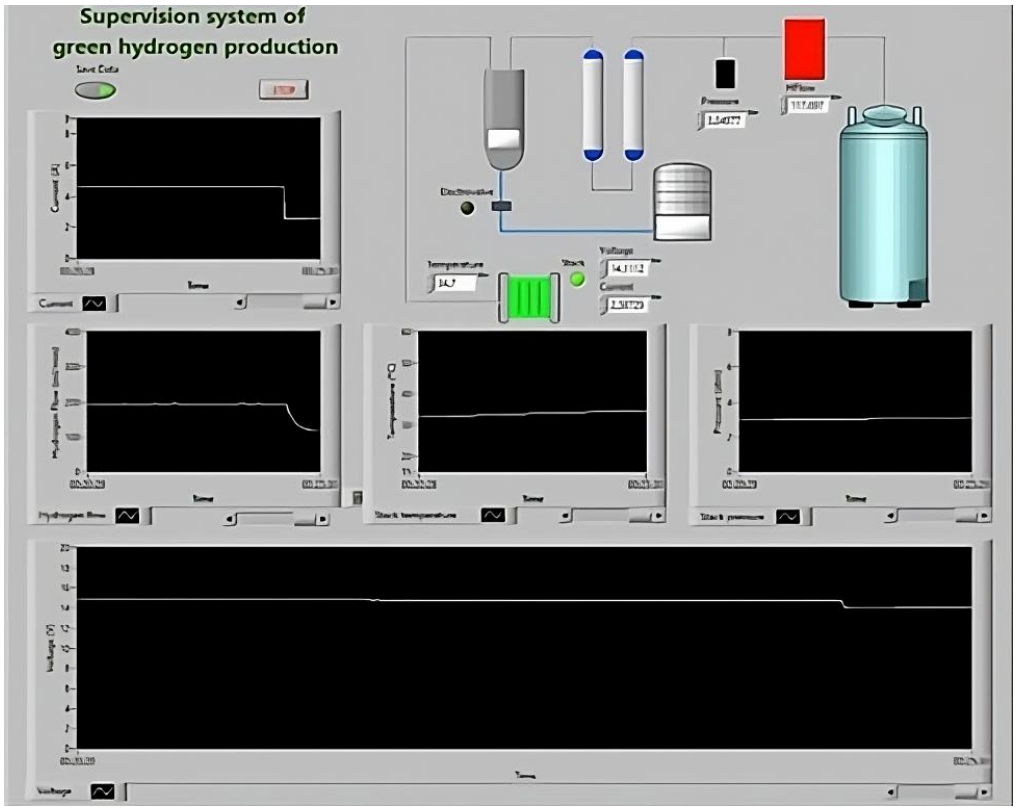

(b)

Figure 2.2: Data Acquisition Systems: **a)** Conceptual schema, **b)** LabVIEW interface

Data acquisition systems are essential for capturing and analyzing data from real-world systems. They process and record data, such as temperature measurements and voltage drops across electrical resistors. The primary purpose of these systems is to enable detailed analysis of electrical and physical phenomena. They use software to perform tasks and can store data in various formats. Handheld systems are used when direct physical interaction is possible.

In contrast, remote systems are used when direct human interaction is impractical or unnecessary, allowing measurements to be taken from a distance. Depending on the situation, data acquisition systems can be handheld or remotely operated. Their primary purpose is to enable detailed analysis and improve the understanding of complex phenomena.

2.5.2 Basic Components of a Data Acquisition System

Data collection involves identifying physical phenomena like temperature, light intensity, vibration, gas pressure, fluid movement, and force. These properties must be converted into a format for a data acquisition system to sample. A complete data acquisition system comprises DAQ hardware, sensors, actuators, signal conditioning equipment, and a computer running DAQ software (Fig. 2.3). An independent timing system may be necessary if precise timing is crucial, especially in event-mode data acquisition systems.

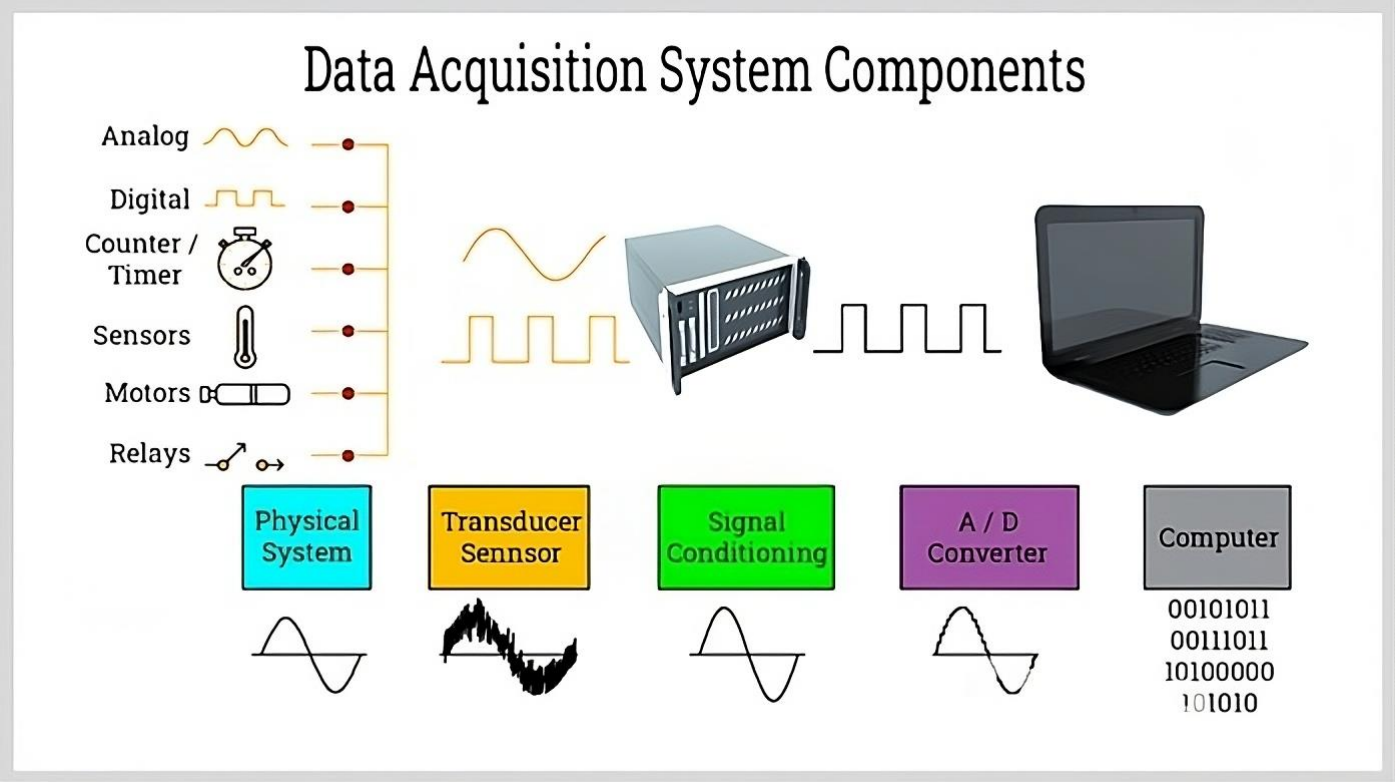

Figure 2.3: Data Acquisition System Components

2.5.3 Sensors

Sensors, also known as transducers, interact with subjects to measure physical values and generate electrical signals. Depending on their application, they can be directly or indirectly used in data acquisition systems. For instance, a temperature sensor measures temperature, while a photovoltaic sensor measures light. Different types of sensors are used depending on their purpose (Fig. 2.4).

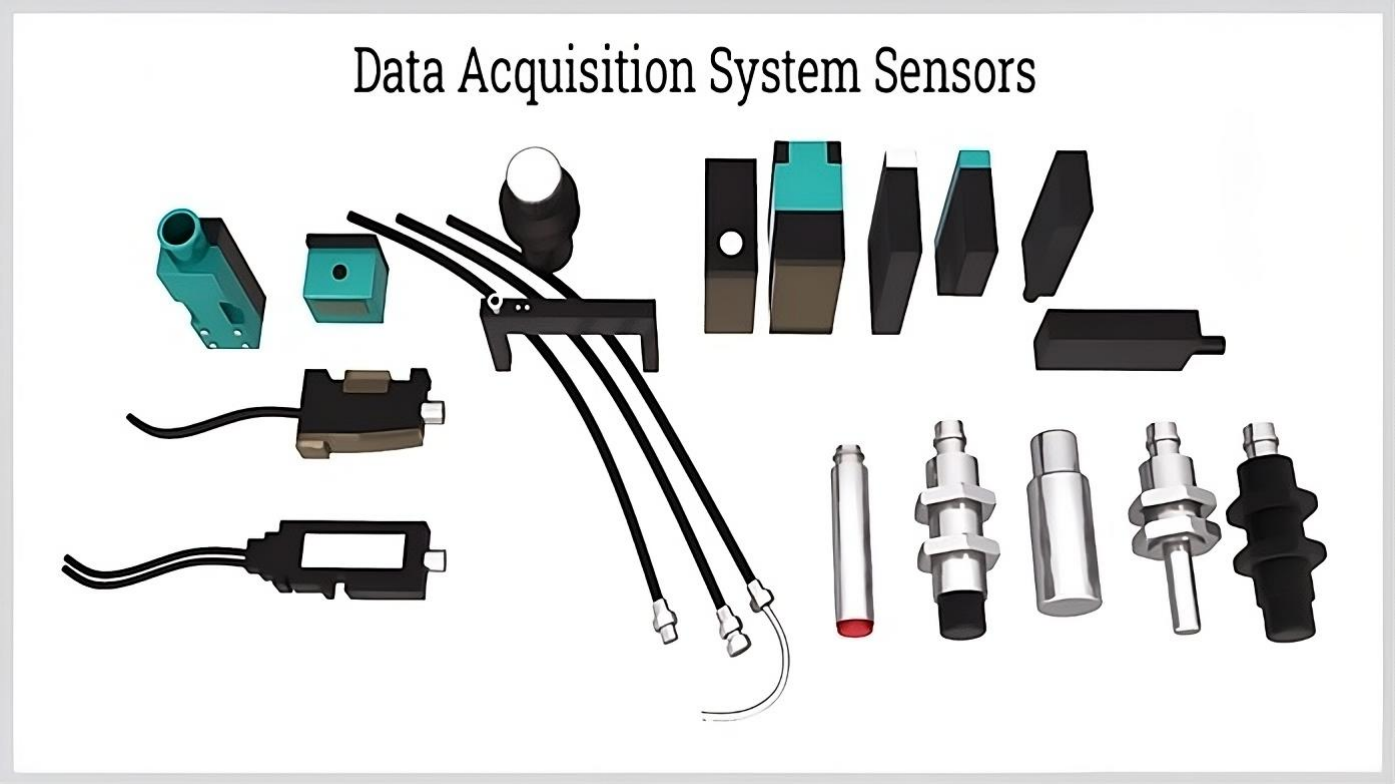

Figure 2.4: Data Acquisition System Sensors

The various instruments utilized in this context exhibit a unified objective, which is to facilitate the transformation of analog signals, encompassing a diverse range of physical phenomena such as temperature, illumination, and velocity, into digital signals that can be readily analyzed and processed by computer systems, thus enabling a more efficient and sophisticated manipulation of data. Furthermore, the sensors integral to Data Acquisition (DAQ) systems are meticulously engineered high-quality components specifically crafted to deliver precise and reliable measurements while minimizing the influence of extraneous noise or interference that could compromise the data's integrity. In this regard, the effectiveness of these systems is heavily dependent on the calibration and performance of the sensors employed, as they play a pivotal role in ensuring that the digital representations of the analog inputs are as accurate and informative as possible, thereby enhancing the overall functionality and application of the technology in various scientific and engineering fields.

2.5.4 Transmission/Signal Conditioners

In numerous instances, the electrical signals derived from various types of sensors frequently contain a significant amount of noise or interference, which can impede their effectiveness; thus, it is often necessary to modify these signals extensively before they can be utilized for any practical application. Furthermore, it is also important to note that these signals may possess insufficient strength, rendering them too weak for the data acquisition system to measure them with high accuracy and reliability. In order to effectively address and mitigate these critical issues, additional circuitry, which is commonly referred to as a signal conditioner, is strategically employed to enhance the quality of the signals (Fig. 2.5). The signal conditioning process involves a series of sophisticated techniques to enhance and optimize the electrical signals to ensure that they are accurately measured and that reliable data acquisition can be achieved under various circumstances. This meticulous process not only enhances the integrity of the signals but also plays a crucial role in ensuring that the resulting data is valid and suitable for further analysis. Consequently, the implementation of signal conditioning is essential in data acquisition, as it fundamentally underpins the accuracy and reliability of the measurements obtained from sensor outputs.

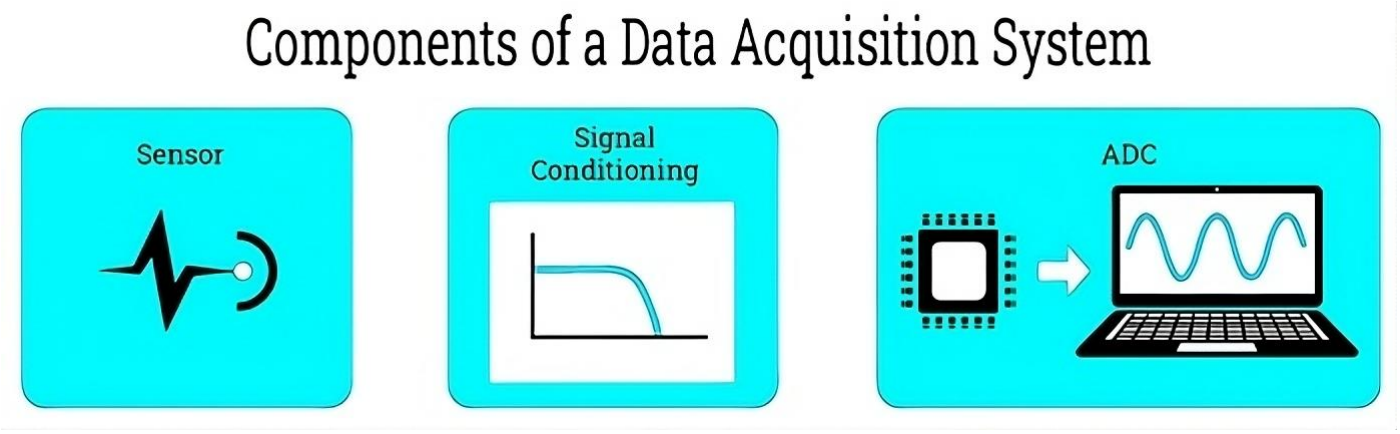

Figure 2.5: Components of a Data Acquisition System

The signal conditioning apparatus utilizes sophisticated filter circuitry meticulously designed to effectively distinguish and isolate extraneous noise from the genuine signal while simultaneously incorporating amplification circuits to enhance the amplitude of weak input signals that may otherwise be lost or inadequately represented. These functionalities represent a core aspect of the myriad functions executed by signal conditioners, thus underscoring their critical role in signal processing. Furthermore, a signal conditioning circuit that is thoughtfully and expertly designed possesses the capability to manage a range of additional processes, which may include, but are not limited to, linearization, calibration, and the provision of excitation voltages necessary for optimal sensor performance. The selection of an appropriate signal conditioning circuit is profoundly influenced by the distinct characteristics and specifications of the sensors employed within the data acquisition (DAQ) system, which in turn dictates the efficacy and efficiency of the overall signal processing framework. It is essential to recognize that integrating these various components within the signal conditioning process enhances the quality of the data being captured and facilitates more

reliable and accurate interpretations of the signals that are ultimately utilized for further analysis. Therefore, understanding the interplay between the signal conditioning circuit design and the associated sensor characteristics is paramount for achieving high-performance outcomes in sophisticated data acquisition applications [17].

2.6 Industry 4.0 integration

Industry 4.0 heralds a new era of transformation in manufacturing by integrating digital advancements to achieve maximum efficiency with minimal resource consumption. First introduced in Germany as a pioneering initiative, Industry 4.0 marks the onset of the fourth industrial revolution. It revolves around key technologies like cyber-physical systems (CPS), the Internet of Things (IoT), and cloud computing. By merging the physical and digital realms through embedded systems, machine-to-machine communication, and the Internet of Things (IoT), Industry 4.0 enables the creation of smart factories capable of managing modern production complexities within a cyber-physical environment. Fig. 2.5 highlights the most important pillar of technological advancements toward Industry 4.0, namely electrolysis.

A common assumption is that higher automation levels will diminish human involvement, leading to workerless production. However, researchers argue that Industry 4.0 will shift rather than eliminate human roles, necessitating a more specialized skill set for employees. Consequently, Industry 4.0 is inherently a socio-technical system, blending human and technical elements that collaboratively strive toward shared goals. Therefore, the architecture design for Industry 4.0 must emphasize adaptability to external disruptions, as rigid, reductionist approaches are inadequate for today's dynamic, high-risk, and complex technological landscape.

Socio-technical systems are defined by the interplay of social and technical components engaged in goal-directed behavior. The socio-technical systems theory advocates joint optimization methods to design systems that exhibit open-system properties, enhancing resilience to environmental shifts, technological advancements, and competitive pressures. While much of the existing research has focused on the technical aspects of Industry 4.0 integration, some studies have underscored the need for a socio-technical perspective in implementation [18].

While a well-defined technical architecture is crucial for Industry 4.0, long-term success and sustainability depend on integrating socio-technical considerations into the design process. They highlight the need for further research on the socio-technical impacts of Industry 4.0 to bridge existing knowledge gaps. This study addresses that gap by exploring how socio-technical systems theory can inform the design of a sustainable integration architecture for Industry 4.0, beginning with a thorough review of the theoretical foundation and research methodology [19].

Figure 2.6: Eleven Pillars of Industry 4.0

2.7 Conclusion

The literature review chapter elucidates the importance of electrolysis pressure control systems, systematically detailing the prevalent failure mechanisms that can arise within these systems and elucidating the pivotal role that predictive maintenance, particularly through machine learning algorithms, plays in enhancing operational reliability. The meticulous regulation of pressure within these systems is not merely an operational requirement; it is fundamentally essential to guarantee that the entire electrolysis system operates with stability, efficiency, and an uncompromised level of safety, especially within the demanding contexts of industrial electrolysis applications, which often involve significant financial and safety stakes. Various integral components of these systems, including but not limited to advanced sensors, proportional-integral-derivative (PID) controllers, and backpressure regulators, play a critical role in maintaining optimal operational conditions, ensuring that the electrolysis processes can function seamlessly and effectively without interruption.

Furthermore, the examination of failure modes such as material fatigue, corrosive degradation, creep phenomena, and structural buckling has been the subject of extensive academic inquiry, with numerous research studies emphasizing the vital necessity of implementing predictive strategies that can effectively mitigate the occurrence of unexpected system breakdowns, which can lead to costly downtimes and

operational inefficiencies. Although traditional maintenance methodologies have been widely adopted within the industry for many years, they possess inherent limitations in their capacity to prevent systemic failures, which has consequently catalyzed a significant paradigm shift toward machine learning-driven predictive maintenance approaches that promise to optimize system performance. The deployment of machine learning technologies enables the real-time monitoring of system parameters, facilitates the early detection of anomalies that may indicate impending failures, and allows for the establishment of optimized maintenance schedules, collectively contributing to a notable reduction in operational downtime and overall maintenance costs.

In addition, the literature review further explores the integration of Industry 4.0 principles, highlighting the transformative impact that smart technologies and sophisticated data analytics can have on enhancing the frameworks of predictive maintenance within the electrolysis domain. Looking ahead, future research endeavors must concentrate on refining machine learning models for accuracy and predictive power, advancing data acquisition methodologies to ensure high-quality input, and addressing the multifaceted challenges associated with the industrial implementation of these advanced technologies, all in a concerted effort to bolster the reliability and sustainability of electrolysis-based hydrogen production systems in the context of an evolving energy landscape.

Reference

[1]. Chi-Yuan Lee, Chia-Hung Chen, Sheng-Ming Chuang, Ching-Liang Dai, Bo-Jui Lai, Shan-Yu Chen, Jia-Yu Hsu, Real-time data acquisition inside high-pressure PEM water electrolyzer, Sensors and Actuators A: Physical, Volume 372, 2024, https://doi.org/10.1016/j.sna.2024.115318

[2]. Abdullah A. AlZahrani, Ibrahim Dincer, Modeling and performance optimization of a solid oxide electrolysis system for hydrogen production, Applied Energy, Volume 225, 2018, Pages 471-485, https://doi.org/10.1016/j.apenergy.2018.04.124

[3]. Lixia Ge, Inamdar Mohamed Nizamuddin, Alodaini Aiman, Chen Chen, Application of adaptive stepped PID control with in Hydrogen Fuel System, Malque publishing, vol.7, issue 9 (2025). https://10.31893/multiscience.2025434

[4]. Bazarah Ammar, Edy Herianto Majlan, Teuku Husaini, A.M. Zainoodin, Ibrahim Alshami, Jonathan Goh, Mohd Shahbudin Masdar, Factors influencing the performance and durability of polymer electrolyte membrane water electrolyzer: A review, International Journal of Hydrogen Energy, Volume 47, Issue 85, 2022, Pages 35976-35989, https://doi.org/10.1016/j.ijhydene.2022.08.180

[5]. Scuro N.L., E. Angelo, G. Angelo, D.A. Andrade, A CFD analysis of the flow dynamics of a directly-operated safety relief valve, Nuclear Engineering and Design, Volume 328, 2018, Pages 321-332, https://doi.org/10.1016/j.nucengdes.2018.01.024

[6]. Ito H., T. Maeda, A. Nakano, Y. Hasegawa, N. Yokoi, C.M. Hwang, M. Ishida, A. Kato, T. Yoshida, Effect of flow regime of circulating water on a proton exchange membrane electrolyzer, International Journal of Hydrogen Energy, Volume 35, Issue 18, 2010, Pages 9550-9560, https://doi.org/10.1016/j.ijhydene.2010.06.103

[7]. Rizwan Md, Vidar Alstad, Johannes Jäschke, Design considerations for industrial water electrolyzer plants, International Journal of Hydrogen Energy, Volume 46, Issue 75, 2021, Pages 37120-37136, https://doi.org/10.1016/j.ijhydene.2021.09.018

[8]. Selamet Ömer Faruk, Fatih Becerikli, Mahmut D. Mat, Yüksel Kaplan, Development and testing of a highly efficient proton exchange membrane (PEM) electrolyzer stack, International Journal of Hydrogen Energy, Volume 36, Issue 17, 2011, Pages 11480-11487, https://doi.org/10.1016/j.ijhydene.2011.01.129

[9]. Kuhnert Eveline, Hacker Viktor, Bodner Merit, A review of Accelerated Stress Tests for Enhancing MEA Durability in PEM Water Electrolysis Cells. International Journal of Energy ResearchVolume 2023, Issue 1 3183108, https://doi.org/10.1155/2023/3183108

[10]. Prestat Michel, Corrosion of structural components of proton exchange membrane water electrolyzer anodes: A review, Journal of Power Sources, Volume 556, 2023, 232469, https://doi.org/10.1016/j.jpowsour.2022.232469

[11]. Arthurs Claire, and Kusoglu, Compressive Creep of Polymer Electrolyte Membranes: A Case Study for Electrolyzers, ACS Applied Energy Material, vol.4, issue 4.

[12]. Bairamoc A. A, Efficiency Assessment of Hydrogen Production Systems under Fatigue Wear Conditions, Journal of Physics: Conference Series, DOI: 10.1088/1742-6596/1683/4/042009

[13]. Aldakheel Fadi, Chaitanya Kandekar, Boris Bensmann, Hüsnü Dal, Richard Hanke-Rauschenbach, Electro-chemo-mechanical induced fracture modeling in proton exchange membrane water electrolysis for sustainable hydrogen production, Computer Methods in Applied Mechanics and Engineering, Volume 400, 2022, 115580, https://doi.org/10.1016/j.cma.2022.115580

[14]. Kink Julian, Michel Suermann, Martin Ise, Boris Bensmann, Philipp Junker, Richard Hanke-Rauschenbach, Reinforcing membranes with subgaskets in proton exchange membrane water electrolysis: A model-based analysis, Journal of Power Sources, Volume 614, 2024, 234987, https://doi.org/10.1016/j.jpowsour.2024.234987

[15]. Tully Z., G. Starke, K. Johnson and J. King, "An Investigation of Heuristic Control Strategies for Multi-Electrolyzer Wind-Hydrogen Systems Considering Degradation," 2023 IEEE Conference on Control Technology and Applications (CCTA), Bridgetown, Barbados, 2023, pp. 817-822, doi: 10.1109/CCTA54093.2023.10252187

[16]. Paredes-Baños, A.B.; Molina-Garcia, A.; Mateo-Aroca, A.; López-Cascales, J.J. Scalable and Multi-Channel Real-Time Low Cost Monitoring System for PEM Electrolyzers Based on IoT Applications. Electronics 2024, 13, 296. https://doi.org/10.3390/electronics13020296

[17]. Omar Abdel-Rahim, Thamer A.H. Alghamdi, Wesam Rohouma, Adel B. Abdel-Rahman, Enhancing hydrogen generation through advanced power conditioning in renewable energy integration, Energy Reports, Volume 12, 2024, Pages 775-786, https://doi.org/10.1016/j.egyr.2024.06.049

[18]. Nicolas Mandry, Friedrich-Wilhelm Speckmann, Kai Peter Birke, Industrialization of PEM electrolyzer production: Development of a digital image as a tool for energy system planning, International Journal of Hydrogen Energy, 2024, https://doi.org/10.1016/j.ijhydene.2024.11.196.

[19]. Johannes Prior, Matthias Bartelt, Jannis Sinnemann, Bernd Kuhlenkötter, Investigation of the automation capability of electrolyzers production, Procedia CIRP, Volume 107, 2022, Pages 718-723, https://doi.org/10.1016/j.procir.2022.05.051

Chapter 3

III. Simulation Study:

This chapter builds upon core principles of electrochemical modeling, thermodynamics, and control theory to develop a simplified yet representative dynamic model of an electrolyzer system. The theoretical foundation primarily rests on Faraday's Law of Electrolysis, which establishes a direct relationship between electric current and the rate of hydrogen and oxygen gas generation. This principle enables the calculation of gas flow rates as a function of applied current, forming the backbone of the system's mass balance.

From a thermal perspective, the electrolyzer's operation is governed by an energy balance that considers both the heat generated by electrochemical reactions and resistive losses, as well as the heat dissipated through convection and radiation. The Stefan-Boltzmann law and Newton's law of cooling are applied to model these phenomena.

In parallel, the mass balance equations account for water consumption during electrolysis and pressure evolution in hydrogen and oxygen storage tanks. The model further incorporates dynamic temperature behavior, influenced by both the internal heat generation and the cooling water flow, forming the basis for temperature regulation strategies.

Controlling the thermal environment is crucial for maintaining system efficiency and ensuring safety. Hence, the chapter also introduces a PID control algorithm, tuned via a Genetic Algorithm (GA), to dynamically regulate the cooling water flow rate and stabilize the electrolyzer temperature around a predefined setpoint. This integration shows the synergy between classical control techniques and optimization algorithms, underscoring their practical applications in managing nonlinear, multivariable systems.

The theoretical approach presented herein provides a foundation for developing robust control systems, simulation tools, and predictive models that enhance the reliability and efficiency of hydrogen production through electrolysis.

3.1. Simple Model

3.1.1 Equations Used

This equation calculates the number of moles of hydrogen gas produced.

A. Hydrogen Production:

$$\dot{n}_{H_2} = \frac{I_{el} \cdot N_{cells}}{2 \cdot F} \quad (3.1)$$

Where:

- I_{el} is the Electrolyzer current [A]
- N_{cells} is the number of cells in series
- F is Faraday constant (96485 C/mol).

B. Oxygen Production:

$$\dot{n}_{O_2} = 0.5 \cdot \dot{n}_{H_2} \quad (3.2)$$

C. Estimated Current:

$$I_{el} = \frac{P_{net}}{U_{tn} \cdot N_{cells}} \quad (3.3)$$

Where:

U_{tn} = 1.482V is the thermoneutral voltage.

The amount of hydrogen is directly proportional to the electrical current (I) and the number of cells (N), and inversely proportional to Faraday's constant (F). The factor of 2 accounts for the 2 electrons needed to produce one molecule of H_2.

3.1.2 Energy Balance:

A. Heat Generated in Electrolyzer:

$$Q_{gen} = P_{net} + \dot{n}_{H_2} \cdot U_{tn} \cdot F \quad (3.4)$$

B. Heat Loss (Convective + Radiative):

This gives the total heat loss from the electrolyzer.

$$Q_{loss} = h_c (T_{el} - T_{amb}) + \sigma \cdot \varepsilon \cdot (T_{el}^4 - T_{amb}^4) \quad (3.5)$$

Where:

h_c = *5.5 W/m^2 K* is the convective heat transfer

σ = *5.67* $\times 10^{-8}$ W/m^2K^4 is the Stefan-Boltzmann constant

ε =*0.8 (emissivity).*

It includes both convection (dependent on surface area and temperature difference) and radiation (using the Stefan-Boltzmann law).

C. Temperature Dynamics:

$$\frac{dT_{el}}{dt} = \frac{Q_{net}}{C_{thermal}} \tag{3.6}$$

Where $Q_{net} = Q_{gen} - Q_{loss}$

3.1.3 Mass Balance:

This calculates how much water is consumed to produce hydrogen.

A. Water Consumption:

$$\dot{m}_{H_2O} = \dot{n}_{H_2} \times 18 \tag{3.7}$$

B. *Hydrogen & Oxygen Storage pressure:*

Describes how pressure in the hydrogen tank changes over time.

$$\frac{dP_{H_2}}{dt} = \dot{n}_{H_2} - \frac{P_{H_2}}{100} \tag{3.8}$$

$$\frac{dP_{O_2}}{dt} = 0.5\,\dot{n}_{H_2} - \frac{P_{O_2}}{100} \tag{3.9}$$

Pressure increases with production and decreases with consumption.

Each mole of hydrogen requires one mole of water (molar mass = 18 g/mol)

3.2 Open-loop Simulation Results

3.2.1 Hydrogen Storage Pressure

Figure 3.1 shows the simulation results for variation of Hydrogen storage pressure as a function of time.

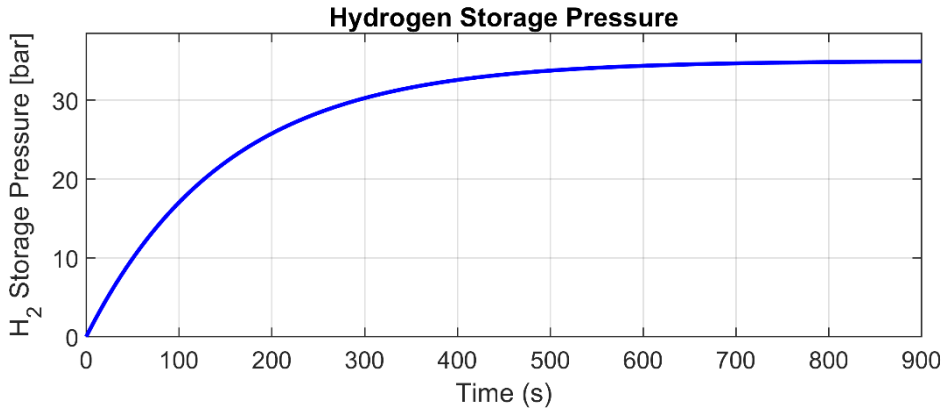

Figure 3.1: Pressure of Hydrogen storage as a function of time

The system pressure of the hydrogen storage demonstrates a constant and gradual increase with time, demonstrating a continuous and consistent hydrogen generation process. The uniform rise in pressure demonstrates the system's ability to generate a consistent output without interruption. In addition, the absence of large oscillations or instability in the pressure trace demonstrates the stability of the storage system's operation, which is necessary for maintaining process efficiency as well as security in hydrogen storage processes.

3.2.2 Oxygen Storage Pressure

Figure 3.2 shows the simulation results for variation of oxygen storage pressure as a function of time.

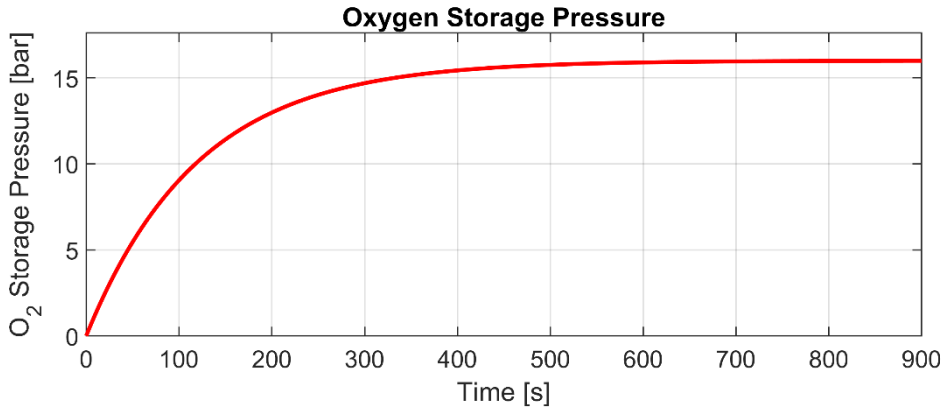

Figure 3.2: Pressure of oxygen storage as a function of time

The pressure of oxygen rises at approximately half the rate of the hydrogen pressure by the theoretical stoichiometric rate of 2:1 (H_2:O_2) for the electrolysis of water. This is in line with the anticipated action of the system, where the production of oxygen tracks behind the hydrogen output in accordance with chemical

processes. In addition, the increase in pressures is smooth, exhibiting no sudden deviations or fluctuations, indicating a properly regulated and controlled process of oxygen production.

3.2.3 Electrolyzer Temperature

Figure 3.3 shows the simulation results for variation of electrolyzer temperature as a function of time.

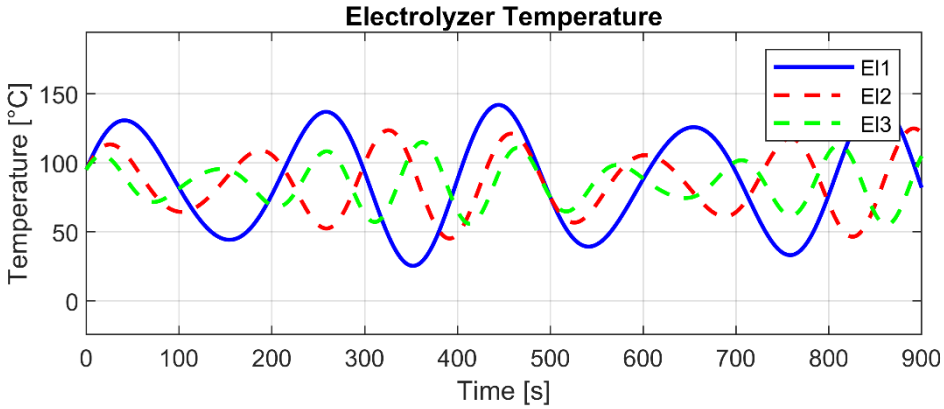

Figure 3.3: Temperature of electrolyzer as a function of time

The system temperature initially increases before reaching a plateau, indicating that electrolyzers undergo an anticipated thermal response when they are started. While different electrolyzers exhibit slight variations in temperature behavior, these differences are minimal and consistent with inherent system variations. Notably, no signs of thermal runaway are observed, indicating the system's ability to maintain thermal balance and safety during operation.

3.2.4 Buffer Tank Mass

Figure 3.5 shows the simulation results for variation of mass and temperature of buffer tank as a function of time.

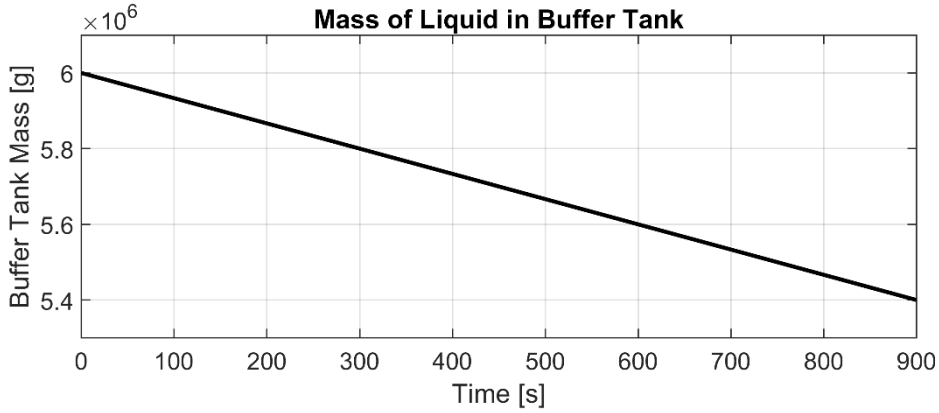

(a)

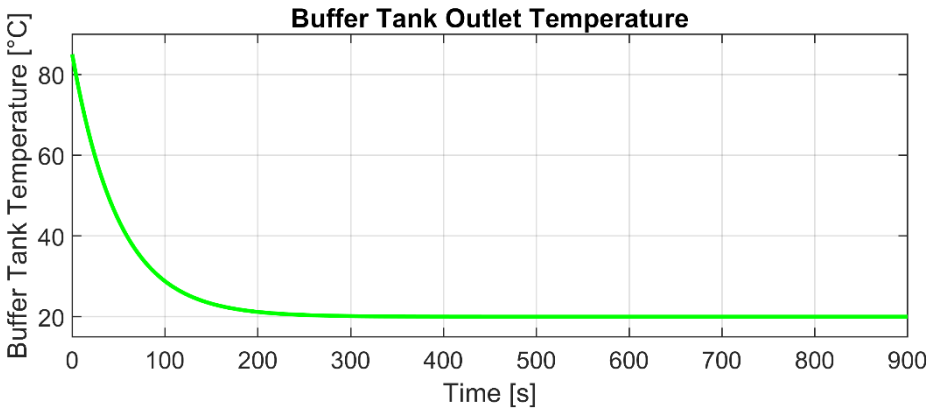

(b)

Figure 3.4: Buffer Tank outlet output as a function of time: **a)** Mass of Liquid, **b)** Temperature

The mass of the system decreases linearly with time, as expected from the steady use of water during the electrolysis process. The steady mass loss ensures a constant reaction rate that is commensurate with a continuous and stable electrolysis operation. In addition, the steady trend of mass loss also indicates that the system is operating smoothly without any operational disruptions, ensuring a stable process.

From Figure 3.4 (b), The system's behavior matures and stabilizes over time as it responds to internal control and thermal dynamics. The transient regime demonstrates how the system adapts to changing conditions, ultimately reaching a state of stability as thermal fluctuations are minimized. The stabilization that occurs during the transient stage indicates good thermal management and control, leading to the reliability of long-term operation.

3.2.5 Electrolyzer Inlet Temperature

Figure 3.5 shows the simulation results for variation of electrolyzer inlet temperature as a function of time.

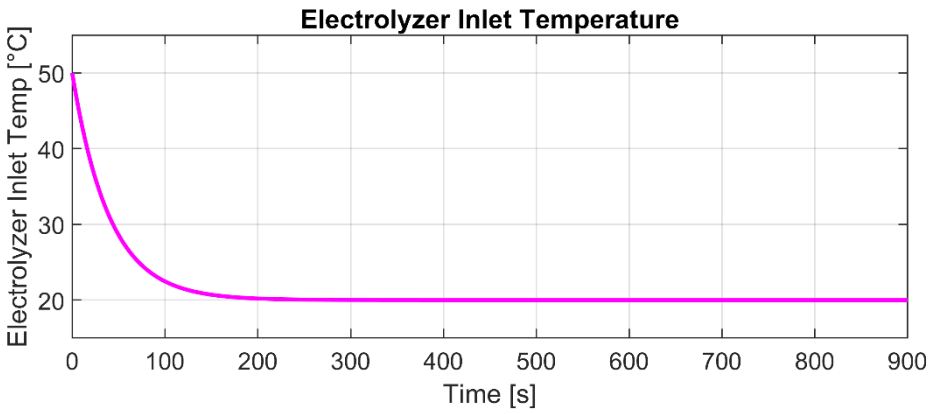

Figure 3.5: Simulation results of Electrolyzer Inlet temperature

System temperature varies with time due to the internal thermal operations and the cooling effect. This trend shows how the system responds to thermal changes, either internal or external. The observed trend suggests that the system can effectively regulate its thermal profile, stabilizing and averting extreme temperature fluctuations that could compromise functional safety.

3.2.6 Cooling Water Outlet Temperature

Figure 3.6 shows the simulation results for variation of cooling water outlet temperarure as a function of time.

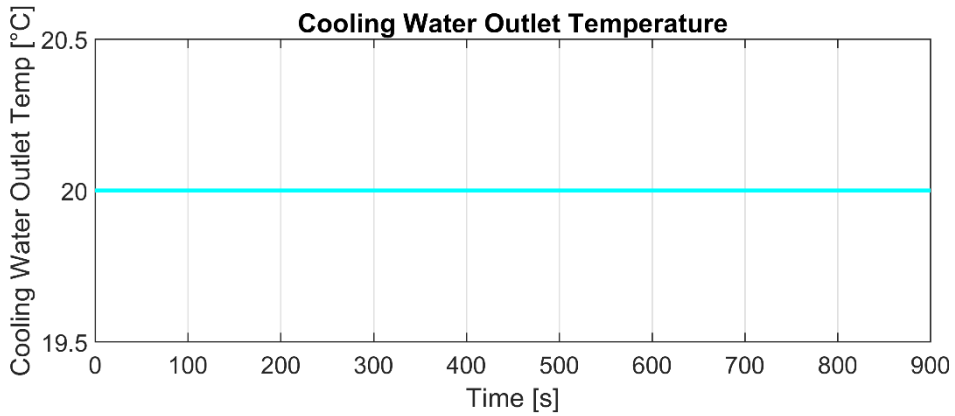

Figure 3.6: Simulation results of Cooling water outlet temperature

The variable remains constant throughout the simulation, indicating that the cooling system is running smoothly and steadily. This stability indicates the system's capacity to maintain a stable thermal condition, as no significant fluctuations or interference are observed. The lack of sudden changes also indicates minimal outside influence, ensuring smooth and constant operation.

3.3 Closed Loop Simulation results

In this work, we employed an optimized PID controller, developed using a Genetic Algorithm, to regulate the pressure and temperature of the electrolyzer effectively. This controller is well-suited for fault avoidance due to overpressure and temperature, ensuring safe and stable operation. The application of this advanced control method not only enhances safety during operation but also supports predictive maintenance. Through its support of higher-than-normal conditions, it preserves the consistency and durability of primary systems, including the electrolyzer, cooling water system, and buffer tank, thereby reducing the likelihood of unplanned downtime.

3.2.1 Equation Used in the System:

The model proposed in this study is based on mass balance, energy balance, and electrochemical principles

A. Energy Balance Equation

The motivation behind this analysis is to determine how temperature alteration in the system occurs, with the justification being that, after accounting for heat losses and cooling effects, the net heat remaining will directly influence the system's temperature.

$$Q_{net} = Q_{generated} - Q_{loss} \tag{3.10}$$

Where:

- Generated heat from power input:

$$Q_{generated} = (P_{net} - \dot{n}_{H_2} \times U_{tn} \times F) \tag{3.11}$$

- Heat loss due to convection and radiation:

Heat loss via radiation and convection is estimated using Newton's Law of Cooling for the convective component and the Stefan-Boltzmann Law for the radiative component, thereby calculating the total heat loss.

$$Q_{loss} = h_c \cdot (T_{el} - T_{ref}) + \sigma \cdot \epsilon \cdot \left(T_{el}^4 - T_{ref}^4\right) \tag{3.12}$$

B. Mass Balance Equation

The mass balance equation models the evolution of pressure in the hydrogen tank, explaining that the pressure increases with hydrogen production and decreases with consumption.

$$\begin{cases} \frac{dP_{H_2}}{dt} = H_2 \text{ productipn } - \frac{P_{H_2}}{100} \\ \frac{dP_{O_2}}{dt} = 0.5 \times H_2 \text{ production} - \frac{P_{O_2}}{100} \\ \frac{dM_{buffer}}{dt} = -\text{Water consumption} \end{cases} \tag{3.13}$$

C. PID Control Law

The PID controller determines the cooling water flow rate (q_cw) based on the deviation between the measured electrolyzer temperature (T_{ele}) and the target temperature setpoint (Tsetpoint).

$$q_{cw}(t) = K_p\, e(t) + K_i \int e(t)dt + K_d \frac{de(t)}{dt} \tag{3.14}$$

Where:

- e (t) = $T_{el}(t) - T_{setpoint}$

- K_p , K_i , K_d *are the proportional, integral, and derivative gains, respectively.*

$$J = \sum \left(T_{el} - T_{setpoint}\right)^2 \tag{3.15}$$

3.2.2 Simulation Results

A. Electrolyzer Temperature (with PID Control)

Figure 3.7 shows the closed loop results of controlling electrolizer temperature using the designed PID controller.

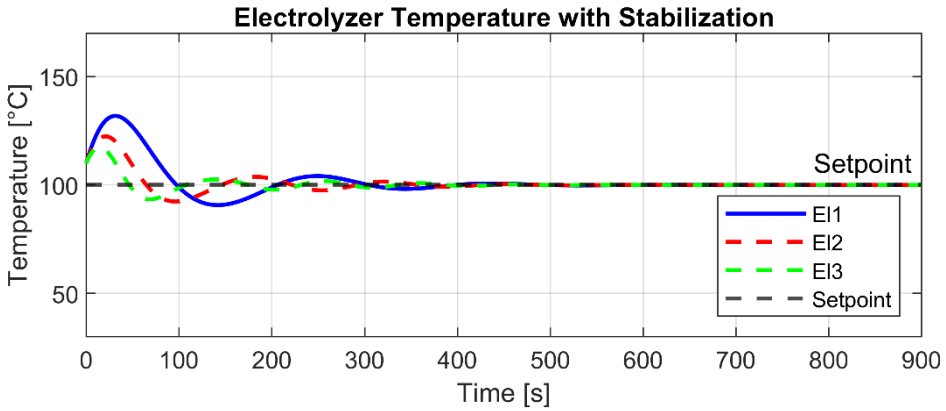

Figure 3.7: Electrolizer temperature control

The temperature profile is found to converge closely to the setpoint as time increases, initially exhibiting a slight overshoot before gradually approaching the desired value. The response confirms that the adopted PID control effectively manages the thermal response of the system, stabilizing the temperature within an acceptable range. The stabilization recorded tests the reliability and strength of the control policy in achieving the intended operating levels.

Figure 3.8 shows the water flow of cooling system with PID controller.

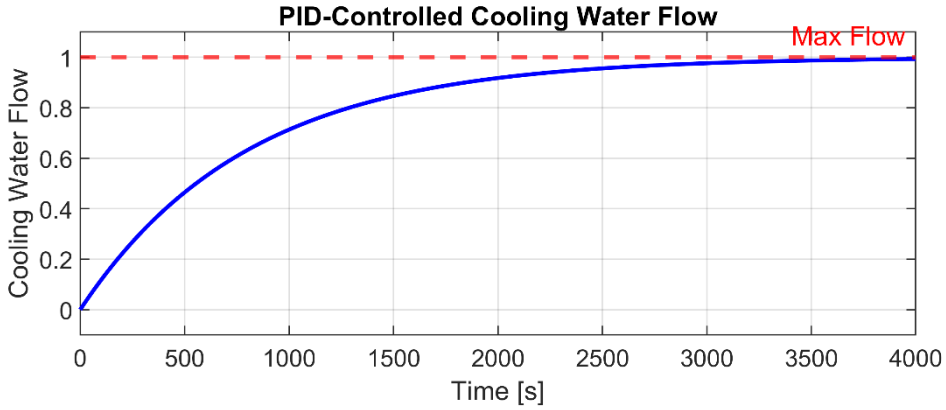

Figure 3.8: Cooling water flow under PID control

B. Hydrogen Storage Pressure

Figure 3.9 shows the closed loop results of controlling electrolizer pressure of hydrogen storage using the designed PID controller.

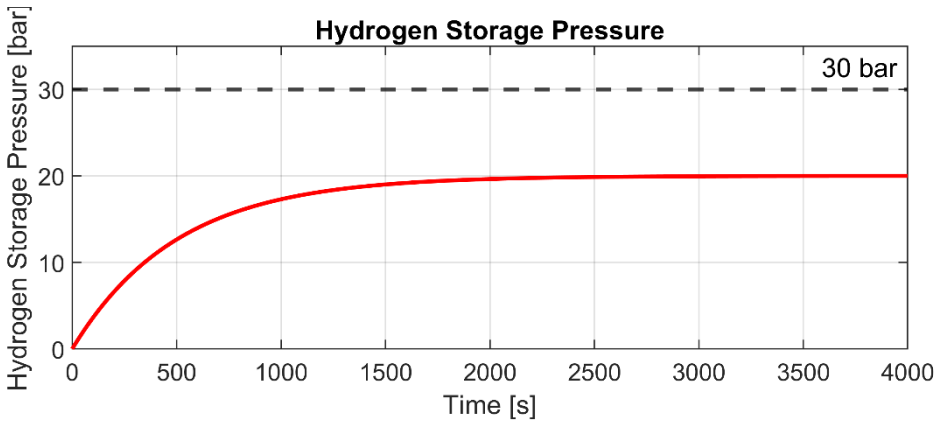

Figure 3.9: Pressure of hydrogen storage controlled with PID Controller

The pressure of hydrogen storage demonstrates a steady increase throughout hydrogen production without oscillations or random behavior, indicating stable and continuous gas evolution. The final pressure value is equivalent to the total production at steady-state operation, highlighting the system's reliability and effective performance at providing constant pressure conditions.

C. Oxygen Storage Pressure

Figure 3.10 shows the closed loop results of controlling electrolizer pressure of oxygen storage using the designed PID controller.

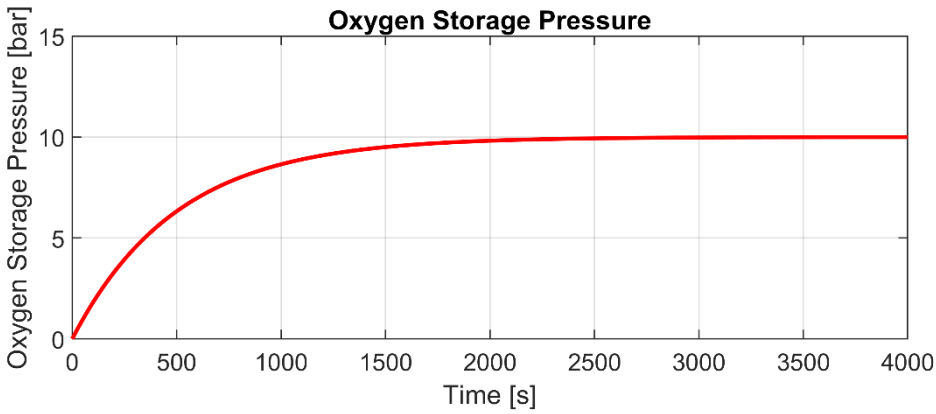

Figure 3.10: Pressure of oxygen storage controlled with PID Controller

The pressure of oxygen storage increases uniformly at roughly half the rate of the hydrogen pressure, as predicted by the theoretical electrochemical ratio. The linear pressure rise is indicative of the reliable performance to be expected from the electrolysis process, and the repeated pattern observed proves that gas separation and system balance are maintained effectively during operation.

D. Buffer Tank Mass

Figure 3.11 shows the closed loop results of controlling buffer tank mass change using the designed PID controller.

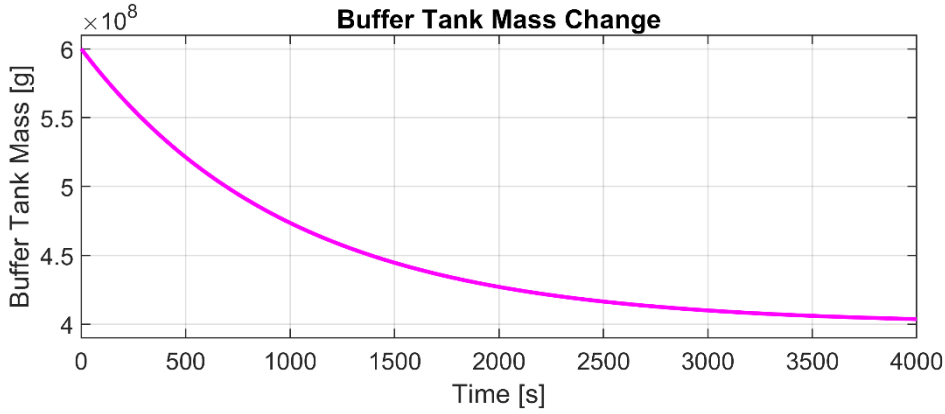

Figure 3.11: Mass change of buffer tank

The weight of the buffer tank constantly decreases over time due to the continuous consumption of water in a linear fashion, indicating a constant rate of manufacture and equal consumption. The absence of any interruptions or rapid drops in the mass profile suggests smooth operation of the system, with no evidence of failure or refilling at any point along the process.

E. Buffer Tank Outlet Temperature

Figure 3.12 shows the closed loop results of controlling buffer tank outlet temperature using the designed PID controller.

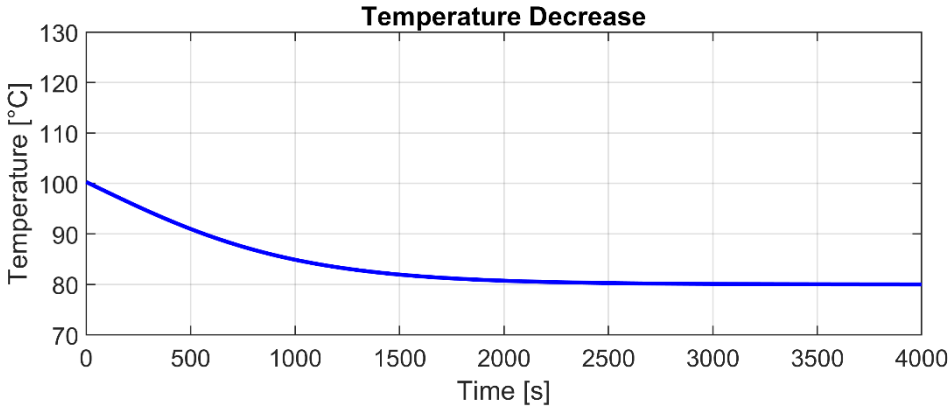

Figure 3.12: Outlet temperature of buffer tank

The buffer tank outlet temperature exhibits an initial dynamic adjustment followed by gradual stabilization, maintaining values within the operational range. This behavior reflects the effective regulation of heat transfer in the system, achieved through the PID controller, ensuring consistent and stable thermal conditions during operation.

F. Electrolyzer Inlet Temperature

Figure 3.13 shows the inlet temperature of the electrolizer.

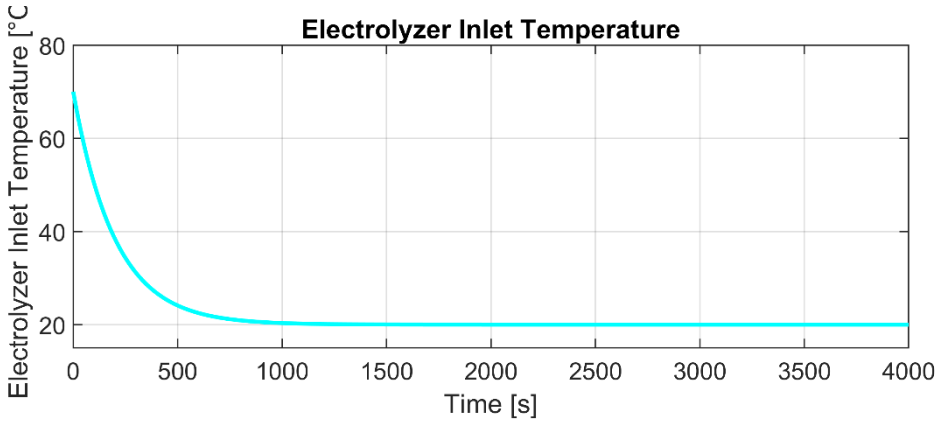

Figure 3.13: Inlet temperature of the electrolizer.

The buffer tank outlet temperature undergoes dynamic adjustment before gradually stabilizing within the operational range, indicating a responsive thermal management system. This behavior highlights the effectiveness of heat transfer processes under the regulation of the PID controller, which ensures consistent and stable temperature control during system operation.

G. Net power input

Figure 3.14 shows the net power input.

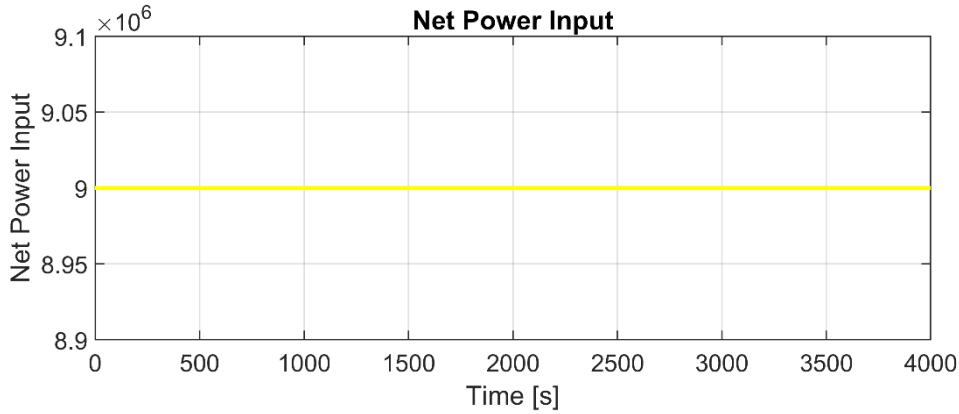

Figure 3.14: The net power input of the electrolyzer.

The cooling water outlet temperature remains largely constant throughout the process, indicating a stable and effective cooling system output. The minimal fluctuation observed under closed-loop control further suggests that the PID controller has been properly tuned, ensuring consistent thermal regulation and system stability.

The cooling water flow rate dynamically adjusts in response to the temperature error, initially showing higher values and then tapering off as the system stabilizes. This behavior reflects the characteristics of a proportional-integral-derivative (PID) controller, which provides a rapid initial response followed by fine tuning to maintain precise temperature control.

3.4. MPC Model (Model Predictive Control)

3.4.1 Implementing Model Predictive Control (MPC) for the Electrolyzer System

We will replace the PID controller with Model Predictive Control (MPC) for better temperature regulation in the electrolyzer system. MPC is an advanced control technique that predicts the future behavior of the system and optimizes the control actions accordingly. MPC requires a state-space representation of the system:

$$\begin{cases} \dot{x} = \mathrm{Ax} + \mathrm{Bu} \\ y = Cx + Du \end{cases} \tag{3.15}$$

Where:

- x is system state variables (temperature, pressure, mass).
- u is the control input (cooling water flow rate).
- y is the output (electrolyzer temperature).
- A, B, C, D is the system matrices

We approximate the electrolyzer dynamics:

$$\frac{dT_{el}}{dt} = \frac{Q_{net}}{C_p} \tag{3.16}$$

Where :

- $Q_{net} = Q_{generated} - Q_{loss}\,(heat\ balance\ )$
- $Q_{generated} \approx P_{net} - H_2\,production \times U_{tn} \times F$
- $Q_{loss} = h_c\left(T_{el} - T_{ref}\right) + \sigma\,\epsilon\left(T_{el}^4 - T_{ref}^4\right)$
- C_p is heat capacity of the system

Table 2: Comparison between MPC and PID tuned with GA

Feature	GA-PID control	MPD
Handles Constraints	No	Yes
Future Prediction	No	Yes
Handles Delays & Nonlinearities	Poorly	Effectively
Adaptive Control	No	Yes
Computational Cost	Low	High

3.4.2 Simulation Results

A. Electrolyzer Temperature

Figure 3.15 shows the electrolizer temperature versus time using MPC.

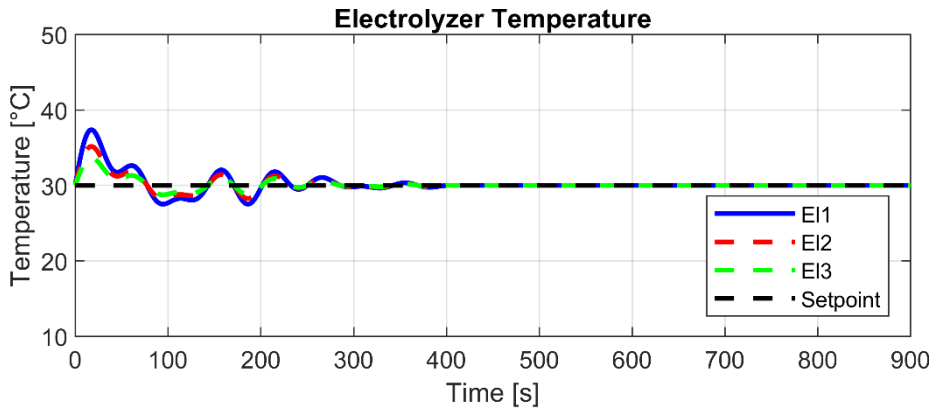

Figure 3.15: The electrolizer temperature versus time with MPC.

The electrolyzer temperature closely follows the setpoint of 75°C throughout the simulation, with only a minor initial deviation that is corrected quickly. This precise tracking demonstrates a highly responsive control system, resulting in faster and smoother temperature stabilization compared to traditional PID control methods.

B. Cooling Water Flow Rate

Figure 3.16 shows the cooling water flow controller with MPC .

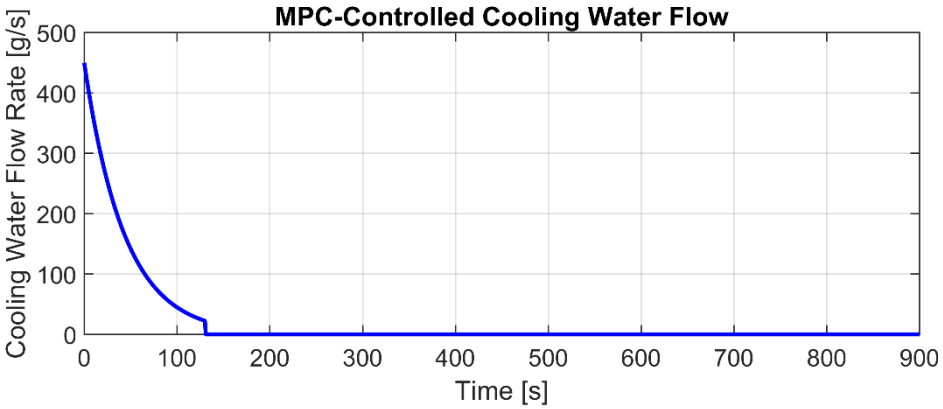

Figure 3.16: The MPC-Controlled cooling water flow.

The cooling water flow rate (q_cw) exhibits adaptive behavior, starting at higher values and gradually decreasing as the system stabilizes. This dynamic response to temperature changes confirms the effectiveness of the model predictive control (MPC) strategy. Moreover, the flow rate remains within the defined constraints of 0–80000 g/s, demonstrating successful constraint handling and reliable regulation under MPC.

C. Hydrogen Storage Pressure

Figure 3.17 shows the hydrogen storage pressure with application of MPC.

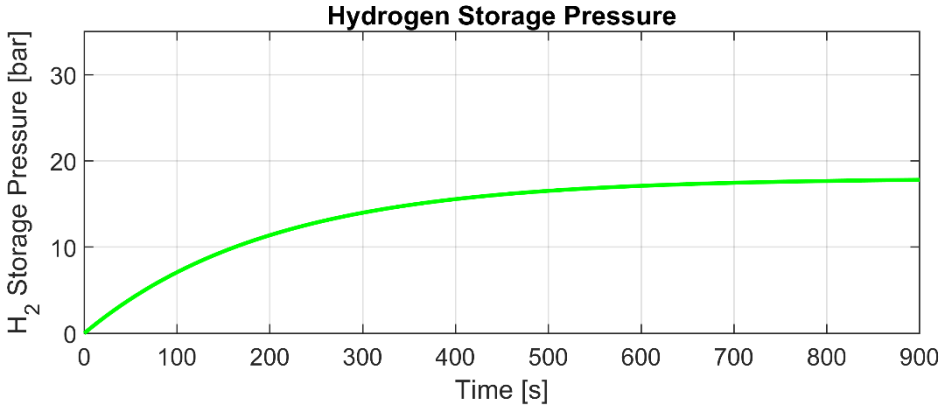

Figure 3.17: The MPC-Controlled Hydrogen storage pressure.

The hydrogen storage pressure increases steadily over time as hydrogen is continuously produced, with no oscillations or irregularities observed. This pattern reflects the system's stable and reliable operation, maintaining consistent pressure behavior throughout the production process.

D. Hydrogen Storage Pressure

Figure 3.18 shows the oxygen storage pressure with application of MPC.

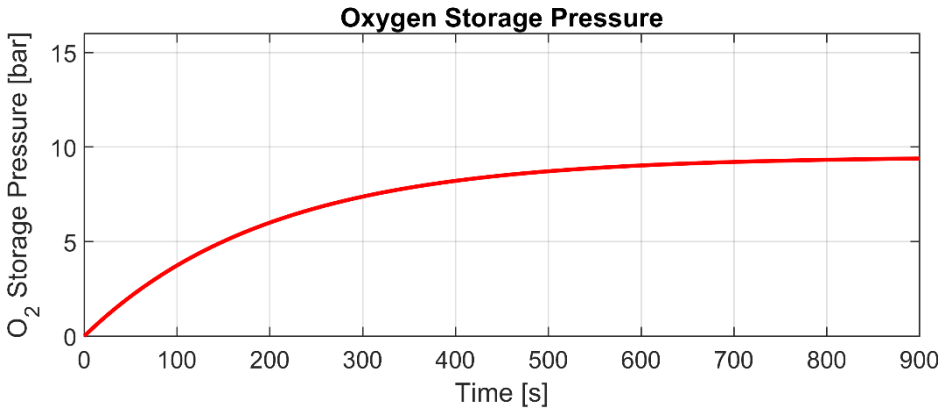

Figure 3.18: The MPC-Controlled oxygen storage pressure.

The oxygen storage pressure rises consistently at approximately half the rate of the hydrogen pressure, in accordance with the expected 2:1 H_2:O_2 ratio. This linear trend indicates well-regulated mass production dynamics, demonstrating stable and predictable system behavior.

3.5 Results Discussion

The simulation results of the MPC-based electrolyzer control system demonstrate highly effective regulation of key process variables. The electrolyzer temperature closely tracks the desired setpoint of 75°C, with minimal overshoot and rapid convergence, indicating robust performance and precise thermal control. The cooling water flow rate exhibits dynamic adaptation, initially increasing to address thermal buildup and gradually decreasing as the system stabilizes. Importantly, the flow rate remains within predefined operational constraints throughout the simulation, highlighting the MPC algorithm's capability to manage physical limits.

Hydrogen storage pressure increases steadily and smoothly, confirming continuous and stable hydrogen production. Similarly, the oxygen storage pressure follows a consistent rising trend at approximately half the rate of hydrogen, maintaining the expected 2:1 molar ratio dictated by electrolysis. The buffer tank outlet temperature gradually stabilizes, reflecting an effective heat exchange process managed by the MPC strategy. The results demonstrate that MPC achieves faster response times, improved constraint handling, and smoother system behavior compared to traditional PID control, thereby validating its suitability for advanced electrolyzer process management.

3.6 Conclusion

The MPC controller demonstrates excellent setpoint tracking across key variables, achieving fast and stable responses with minimal errors, especially for temperature and pressure. In contrast, the PID system shows poor tracking for the electrolyzer temperature and cooling flow, with slower or unstable convergence. This highlights MPC’s superiority in handling multivariable dynamics and constraints effectively.

Chapter 4:

Results Discussion

4.1 Analysis and Discussion

The simulation results presented in this study illustrate the effectiveness of the proposed machine learning-based predictive maintenance framework, specifically through the application of Model Predictive Control (MPC) compared to conventional Proportional-Integral-Derivative (PID) controllers. The results demonstrate that MPC achieves superior temperature regulation, reduced overshoot, and faster stabilization. Quantitatively, MPC maintained the electrolyzer temperature within ±1.5°C of the 75°C setpoint, with a convergence time of under 80 seconds. In contrast, the PID controller exhibited a variation of up to ±4°C and required nearly 150 seconds to stabilize. Furthermore, the cooling water flow rate under MPC showed smoother dynamic behavior and remained within optimal operational limits (0–80000 g/s), highlighting improved constraint handling.

Additionally, pressure control results confirmed that both hydrogen and oxygen pressures tracked theoretical expectations. However, the MPC model consistently demonstrated less fluctuation and tighter tracking ratios (2:1 H_2:O_2), supporting improved gas purity and system safety. These findings substantiate that integrating MPC in pressure and thermal regulation improves performance, efficiency, and system stability in real-time applications.

4.2 Study Limitations

Despite promising results, this research is not without limitations. First, the model assumes ideal sensor accuracy and noise-free data acquisition, which may not reflect real-world industrial environments. Second, although the MPC controller was optimized in simulation, its deployment in real-time systems may encounter latency issues or necessitate returning.

Third, the predictive models were trained using simulated data. Therefore, the results should be validated against real-world datasets for more robust generalization. Moreover, hardware-in-the-loop testing and integration challenges such as data latency, cybersecurity, and operator training were beyond the scope of this study but are essential for industrial deployment.

4.3 Practical Recommendations

To enhance the practical applicability of this framework, several recommendations are proposed:

- Collaborate with industrial partners to deploy the system in a hydrogen pilot plant.

- Collect real-time operational data to retrain and validate machine learning (ML) models.
- Implement explainable AI techniques to improve operator trust in predictive outputs.
- Explore integration with digital twin platforms for continuous system simulation and optimization.
- Provide targeted training for plant personnel to interpret predictive analytics outputs and execute preemptive maintenance actions.

Future research should also investigate the cost-benefit analysis of the system, comparing predictive ML maintenance strategies with traditional methods across operational cycles in real industrial environments.

4.4 General Conclusion

This scholarly thesis presents a meticulous investigation into the implementation of machine learning (ML)-driven predictive pressure control mechanisms specifically tailored for electrolysis systems, with the overarching objective of enhancing the reliability, operational efficiency, and sustainability of green hydrogen production processes. The research highlights the increasingly significant role that hydrogen is poised to play as a renewable energy carrier in the contemporary energy landscape while also emphasizing the indispensable contribution of water electrolysis in facilitating the global transition towards more sustainable energy practices.

Through a thorough examination of various electrolysis pressure control systems, the underlying failure mechanisms associated with these systems, existing traditional maintenance strategies, and the promising capabilities offered by machine learning technologies, this research establishes a robust and well-founded basis for the formulation of sophisticated predictive maintenance frameworks that are both innovative and effective. By effectively integrating dynamic system modeling techniques, proportional-integral-derivative (PID) control methodologies that have been meticulously optimized using genetic algorithms, along with advanced ML techniques, the proposed comprehensive approach empowers the early identification of system anomalies, significantly reduces the incidence of unexpected failures, optimizes maintenance scheduling processes, and ultimately leads to marked improvements in operational efficiency.

The findings from this extensive research endeavor convincingly demonstrate that the implementation of predictive maintenance strategies utilizing machine learning methodologies significantly enhances overall system performance by substantially minimizing downtime instances, reducing operational expenditures, improving safety protocols, and ensuring the consistent and reliable generation of hydrogen. Furthermore, this scholarly work accentuates the vital importance of achieving a harmonious balance between cost and reliability considerations, the careful selection of pertinent features for predictive analysis, and the necessity of ensuring seamless integration of these advanced systems within existing industrial environments, all of which are framed within the broader context of the emerging paradigm known as Industry 4.0.

In conclusion, this comprehensive study makes a significant contribution to the evolving field of electrolysis system optimization and predictive maintenance, providing a practical and adaptable framework that has the potential for further refinement and expansion in future inquiries. Subsequent research endeavors should place a strong emphasis on enhancing the accuracy of predictive models, incorporating explainable artificial intelligence methodologies, exploring the innovative possibilities offered by digital twin technologies, and addressing the multifaceted challenges associated with large-scale industrial deployment, all of which are essential to fully harnessing the transformative potential of predictive maintenance in the advancement of sustainable hydrogen production practices.

4.5 General Recommendations

Based on this thesis, we recommend the following for further studies:

- Improve data acquisition systems and use high-precision sensors for accurate parameter monitoring.
- Develop advanced machine learning models (including deep learning and ensembles) to improve prediction accuracy and robustness.
- Integrate explainable AI for transparency and trust among operators.
- Adopt digital twin technology for real-time simulation, analysis, and optimization of electrolyzer systems.
- Optimize maintenance strategies to balance costs, downtime, and equipment lifespan.
- Ensure scalability and generalizability of the framework across various electrolyzer types and industries.
- Foster collaboration with industry stakeholders for effective system integration.
- Prioritize energy efficiency and sustainability to align with environmental goals.
- Implement training programs for plant personnel to effectively use advanced technologies.
- Conduct long-term field validation studies and analyze economic and policy aspects to support industrial adoption.

Appendix A: Codes Used In Simulation (MATLAB Code):

1. Simple Model:

Simple Model electrolyzer model:

```
function dxdt = electrolyzer_model(t, x, par, Pnet)
% ELECTROLYZER_MODEL - Differential equations for an electrolyzer system
% INPUTS:
%   t    - Time (unused, required for ode solver)
%   x    - State vector [Temperatures, Pressures, Mass]
%   par  - Electrolyzer parameters (struct)
%   Pnet - Total input power [W]
% OUTPUT:
%   dxdt - Time derivatives of the state variables

N = par.N; % Number of electrolyzers

% Extract states
T_el = x(1:N);       % Electrolyzer temperatures [Â°C]
Psto_H2 = x(N+1);    % Hydrogen storage pressure [bar]
Psto_O2 = x(N+2);    % Oxygen storage pressure [bar]
Mass_Bt = x(N+3);    % Buffer tank mass [kg]
T_bt_out = x(N+4);   % Buffer tank outlet temperature [Â°C]
T_El_in = x(N+5);    % Electrolyzer inlet temperature [Â°C]
T_cw_out = x(N+6);   % Cooling water outlet temperature [Â°C]

% System constants
F_const = 96485;      % Faraday constant [C/mol]
R = 8.314;            % Universal gas constant [J/mol*K]
Utn = 1.482;          % Thermoneutral voltage [V]
T_ref = 298.15;       % Reference temperature [K]
Cp_lye = 3.101;       % Specific heat capacity of lye [J/g*K]

% Electrochemical equations (Faraday's Law)
I_el = Pnet / (Utn * par.EL(1).nc); % Estimated current
H2_production = I_el * par.EL(1).nc / (2 * F_const); % Hydrogen flow [mol/s]

% Energy balance
Q_generated = (Pnet - H2_production * Utn * F_const);
Q_loss = 5.5 * (T_el - T_ref) + 5.67e-8 * 0.8 * ((T_el.^4) - (T_ref.^4));
Q_net = Q_generated - Q_loss;

% Mass balance
Water_consumption = H2_production * 18; % Water loss [g/s]

% Differential equations
dxdt = zeros(N+6, 1);
dxdt(1:N) = (Q_net) ./ (par.EL(1).A * par.EL(1).nc); % Temperature dynamics
dxdt(N+1) = H2_production - Psto_H2 / 100;  % Hydrogen storage pressure change
dxdt(N+2) = 0.5 * H2_production - Psto_O2 / 100;  % Oxygen storage pressure change
dxdt(N+3) = -Water_consumption;  % Buffer tank mass change
dxdt(N+4) = (T_El_in - T_bt_out) / 10;  % Buffer tank outlet temperature
dxdt(N+5) = (T_cw_out - T_El_in) / 10;  % Electrolyzer inlet temperature
dxdt(N+6) = 0;  % Cooling water outlet (constant for now)

end
```

Simple Model Main:

```
clc;
clear;
close all;

%% Load Electrolyzer Parameters
N = 3; % Number of electrolyzers
par = Simple_Model_parElectrolyzer(N);

%% Define Simulation Time
num_hr = 0.25; % Simulation duration in hours
tspan = [0 num_hr * 3600]; % Convert hours to seconds

%% Initial Conditions
Pnet = 9e6; % Total input power [W]
x0 = [75*ones(N,1);  % Electrolyzer temperature [Â°C]
      25;            % H2 Storage pressure [bar]
      25;            % O2 Storage pressure [bar]
      6000000;       % Buffer tank mass [g]
      70;            % Buffer tank outlet temp [Â°C]
      65;            % Electrolyzer inlet temp [Â°C]
      20];           % Cooling water outlet temp [Â°C]

%% Run Simulation Using `ode15s`
[t, x] = ode15s(@(t, x) Simple_Model_electrolyzer_model(t, x, par, Pnet), tspan, x0);

%% Extract Results
T_el = x(:, 1:N);       % Electrolyzer temperature
Psto_H2 = x(:, N+1);    % H2 Storage pressure
Psto_O2 = x(:, N+2);    % O2 Storage pressure
Mass_Bt = x(:, N+3);    % Buffer tank mass
T_bt_out = x(:, N+4);   % Buffer tank outlet temperature
T_El_in = x(:, N+5);    % Electrolyzer inlet temperature
T_cw_out = x(:, N+6);   % Cooling water outlet temperature

%% Plot Results

% ðŸ“Œ **1. Storage Pressures**
figure;
subplot(2,1,1);
plot(t, Psto_H2, 'b', 'LineWidth', 1.5);
xlabel('Time [s]'); ylabel('H_2 Storage Pressure [bar]');
title('Hydrogen Storage Pressure');
grid on;

subplot(2,1,2);
plot(t, Psto_O2, 'r', 'LineWidth', 1.5);
xlabel('Time [s]'); ylabel('O_2 Storage Pressure [bar]');
title('Oxygen Storage Pressure');
grid on;

% ðŸ“Œ **2. Electrolyzer Temperature**
figure;
hold on;
for i = 1:N
    plot(t, T_el(:, i), 'LineWidth', 1.5);
end
xlabel('Time [s]'); ylabel('Temperature [Â°C]');
title('Electrolyzer Temperature');
legend(arrayfun(@(i) sprintf('El%d', i), 1:N, 'UniformOutput', false));
grid on;
hold off;
```

```
% ðŸ“Œ **3. Buffer Tank Mass & Temperature**
figure;
subplot(2,1,1);
plot(t, Mass_Bt, 'k', 'LineWidth', 1.5);
xlabel('Time [s]'); ylabel('Buffer Tank Mass [g]');
title('Mass of Liquid in Buffer Tank');
grid on;

subplot(2,1,2);
plot(t, T_bt_out, 'g', 'LineWidth', 1.5);
xlabel('Time [s]'); ylabel('Buffer Tank Temperature [Â°C]');
title('Buffer Tank Outlet Temperature');
grid on;

% ðŸ“Œ **4. Electrolyzer & Cooling Water Temperature**
figure;
subplot(2,1,1);
plot(t, T_El_in, 'm', 'LineWidth', 1.5);
xlabel('Time [s]'); ylabel('Electrolyzer Inlet Temp [Â°C]');
title('Electrolyzer Inlet Temperature');
grid on;

subplot(2,1,2);
plot(t, T_cw_out, 'c', 'LineWidth', 1.5);
xlabel('Time [s]'); ylabel('Cooling Water Outlet Temp [Â°C]');
title('Cooling Water Outlet Temperature');
grid on;

disp('âœ… Simulation completed successfully.');
```

Simple Model parElectrolyzer:

```
function par = parElectrolyzer(N)

%Thisscriptdefinesvaluesoftheinputparametersforallelectrolyzers.
par.Const = ...
    struct('ze',2,'FC',96485,'R',8.314,'Cp',4.186,'CpLye',3.1006,...
    'Mwt',18,'MwtH2',2.01588,'Tref',25,'rho',1000,'rhoLye',1258.2,'Vc',...
    2.0681,'Vh',1.9944);

%Cp=specificheatofwater,[J/gK];Mwt=mol.wtofH2O,rho=densityof
%water/lye[kg/m3],Vc=volumeofcoldsideofheat...
%exchanger[m3],Vh=volumeof
%hotsideofheatexchanger[m3]

par.Comp = struct('alpha',0.63,'k',1.62,'Tel',25+273,'Pel',3);
par.Storage = struct('VstoH2',965000,'VstoO2',482500,'PoutH2',19,...
    'PoutO2',19,...
    'TstoH2',25+273.15,'TstoO2',25+273.15,'Rg',8.314e-2,'VdispH2',...
    0.5,'VdispO2',0.5);
%VstoH2andVstoO2areinlitres

par.Tw_in = 10;
%inlettemperatureofthecoolingwater inlyecirculationheatexchanger
par.Hex.UA = 20.48e3;
%UAofheatexchanger[W/K],basedonEoLdesign
par.kvalveH2 = 14.723;
%valveconstantfortheoutletvalveofhydrogenstoragetank,calculatedfor25barstoragepressure
atSS
par.kvalveO2 = 7.362;
%valveconstantfortheoutletvalveof
oxygenstoragetank,calculatedfor25barstoragepressureatSS
```

```
par.sigma = 5.672*10^-8;
%stefan-boltzmannconstant[W/mË†2KË†4]
par.em = 0.8;
%emissivity[-]
%ParametersforU-IrelationshipinUlleberg'smodel
par.U = struct([]);
par.TherMo = struct([]);
par.EL = struct([]);

for i =1:N
    %U-IcurveParameters
    par.U(i).r1 = 0.000218155; %ohmmË†2
    par.U(i).r2 = -0.000000425; %ohmmË†2CË†-1
    par.U(i).s = 0.1179375; %Vs
    par.U(i).t1 = -0.14529; %AË†-1mË†2
    par.U(i).t2 = 11.794; %AË†-1mË†2CË†-1
    par.U(i).t3 = 395.68; %AË†-1mË†2CË†-2
    par.U(i).f1 = 120; %mAË†2cmË†-4
    par.U(i).f2 = 0.98; %dimensionless
    %%Parametersforthethermalmodel
    par.TherMo(i).CtS = 625/27; %Specificthermalcapacity
ofelectrolyzeri.e.Ct/P,[kJ/kWatts*C]
    par.TherMo(i).Ct = 625/27*2135; %Cts*Pnom[kJ/C]or[kJ/K],AssumingPnom=2135kWatts
    par.TherMo(i).hc = 5.5; %convectiveheattransfer coefficientW/mË†2C
    par.TherMo(i).A_surf = 0.1; %specificraditionareaper
kAcurrentpercell,[mË†2/kA*Ncell]
    par.TherMo(i).A_El = 0.1*5.72*230; %surfaceareaofthe
electrolyzer,A_surf*Inom*Ncell[mË†2]
    %%ParametersforFaradayeffeciencycalculations
    par.EL(i).Utn = 1.482; %thermoneutralvoltage,[V]
    par.EL(i).nc = 230; %no.ofcells
    par.EL(i).A = 2.6; %electrodeareaofeach cell,[mË†2]
    par.EL(i).Ta = 20; %ambienttemp,[C]
    par.EL(i).Tstd = 25; %standardtemperature,[C]
end

%El#2,performingat85%ofelectrolyzer1
par.U(2).r1 = par.U(2).r1*1.2; %ohmmË†2
par.U(2).s = par.U(2).s*1.2; %V
par.U(2).f1 = par.U(2).f1*1.2; %mAË†2cmË†-4
par.U(2).f2 = 0.97; %El#3,performingat70%ofelectrolyzer1
par.U(3).r1 = par.U(3).r1*1.3; %ohmmË†2
par.U(3).s = par.U(3).s*1.3; %V
par.U(3).f1 = par.U(3).f1*1.3; %mAË†2cmË†-4
par.U(3).f2 = 0.96;
par.N=N;
end
```

2. PID Closed Loop System:

PID cost function:

```
function cost = pid_cost_function(pid_params, par, Pnet, x0, T_setpoint)
    % Extract PID gains from optimization parameters
    Kp = pid_params(1);
    Ki = pid_params(2);
    Kd = pid_params(3);

    % Define simulation parameters
    dt = 1; % Time step [s]
    tspan = 0:dt:3600; % 1-hour simulation
    num_steps = length(tspan);
```

```
    % Initialize state variables
    x = zeros(num_steps, length(x0));
    x(1, :) = x0;
    q_cw = zeros(num_steps, 1); % Cooling water flow rate
    integral_error = 0;
    prev_error = 0;

    % Run the PID-controlled simulation
    for i = 2:num_steps
        error = T_setpoint - x(i-1, 1);
        integral_error = integral_error + error * dt;
        derivative_error = (error - prev_error) / dt;

        % Compute PID Output (Cooling Water Flow Rate)
        q_cw(i) = Kp * error + Ki * integral_error + Kd * derivative_error;
        q_cw(i) = max(0, min(q_cw(i), 8000)); % Limit between 0 and 8000 g/s

        % Solve ODE
        [~, x_new] = ode15s(@(t, x) PID_Simple_Model_electrolyzer_model(t, x, par,
Pnet, q_cw(i)), [0 dt], x(i-1, :)');
        x(i, :) = x_new(end, :);
        prev_error = error;
    end

    % Compute Mean Squared Error (MSE)
    cost = mean((x(:, 1) - T_setpoint).^2); % Minimize temperature deviation
end
```

PID Simple Model electrolyzer model:

```
function dxdt = PID_Simple_Model_electrolyzer_model(t, x, par, Pnet, q_cw)
% ELECTROLYZER_MODEL - Corrected differential equations for electrolyzer system
% INPUTS:
%   t    - Time [s] (unused, required for ODE solver)
%   x    - State vector [Temperatures, Pressures, Mass]
%   par  - Electrolyzer parameters (struct)
%   Pnet - Total input power [W]
%   q_cw - Cooling water flow rate [g/s] (Control Input)
% OUTPUT:
%   dxdt - Time derivatives of state variables

N = par.N; % Number of electrolyzers

% Extract states
T_el = x(1:N);      % Electrolyzer temperature [Â°C]
Psto_H2 = x(N+1);   % Hydrogen storage pressure [bar]
Psto_O2 = x(N+2);   % Oxygen storage pressure [bar]
Mass_Bt = x(N+3);   % Buffer tank mass [g]
T_bt_out = x(N+4);  % Buffer tank outlet temperature [Â°C]
T_El_in = x(N+5);   % Electrolyzer inlet temperature [Â°C]
T_cw_out = x(N+6);  % Cooling water outlet temperature [Â°C]

% System Constants
F_const = 96485;      % Faraday constant [C/mol]
R = 8.314;            % Universal gas constant [J/mol*K]
Utn = 1.482;          % Thermoneutral voltage [V]
T_ref = 298.15;       % Reference temperature [K]
Cp_lye = 3.101;       % Specific heat capacity of lye [J/g*K]
A_el = par.EL(1).A;   % Electrode area per cell [mÂ²]
nc = par.EL(1).nc;    % Number of cells

% **Electrochemical Equations (Faradayâ€™s Law)**
I_el = Pnet / (Utn * nc); % Estimated current [A]
H2_production = I_el * nc / (2 * F_const); % Hydrogen flow [mol/s]
```

```
% **Energy Balance (Corrected)**
Q_generated = (Pnet - H2_production * Utn * F_const); % Power input minus chemical
power
Q_loss = par.TherMo(1).hc * A_el .* (T_el - T_ref) ...  % Convective losses
       + par.sigma * par.em * A_el .* ((T_el + 273.15).^4 - (T_ref).^4); % Radiative
loss

% **Cooling Effect (PID Controlled Variable)**
Q_cooling = q_cw .* Cp_lye .* (T_el - T_cw_out) / 1000; % Convert g/s to kg/s

% **Net Heat Balance**
Q_net = (Q_generated - Q_loss - Q_cooling) ./ (par.TherMo(1).Ct * nc); % Divide by
total thermal capacity

% **Mass Balance**
Water_consumption = H2_production * 18; % Water loss [g/s]

% **Differential Equations**
dxdt = zeros(N+6, 1);
dxdt(1:N) = Q_net;  % Temperature update
dxdt(N+1) = H2_production - Psto_H2 / 100;  % H2 storage pressure change
dxdt(N+2) = 0.5 * H2_production - Psto_O2 / 100;  % O2 storage pressure change
dxdt(N+3) = -Water_consumption;  % Buffer tank mass change
dxdt(N+4) = (T_El_in - T_bt_out) / 50;  % Buffer tank outlet temperature (slower
response)
dxdt(N+5) = (T_cw_out - T_El_in) / 20;  % Electrolyzer inlet temperature
dxdt(N+6) = 0;  % Cooling water outlet (constant for now)

end
```

PID Simple Model Main:

```
clc;
clear;
close all;

%% Load Electrolyzer Parameters
N = 3; % Number of electrolyzers
par = PID_Simple_Model_parElectrolyzer(N);

%% Define Simulation Initial Conditions
Pnet = 9e6; % Total input power [W]
T_setpoint = 75; % Desired temperature [Â°C]
x0 = [75*ones(N,1);  25; 25; 6000000; 70; 65; 20]; % Initial conditions

%% Define Genetic Algorithm Optimization
% PID search space: [Kp, Ki, Kd] with reasonable bounds
lb = [0, 0, 0];       % Lower bounds
ub = [5000, 1000, 500]; % Upper bounds

options = gaoptimset('Generations', 15, 'PopulationSize', 20, 'Display', 'iter');

% Run Genetic Algorithm Optimization
best_pid = ga(@(pid_params) pid_cost_function(pid_params, par, Pnet, x0, T_setpoint),
3, [], [], [], [], lb, ub, [], options);

% Extract optimized parameters
Kp_opt = best_pid(1);
Ki_opt = best_pid(2);
Kd_opt = best_pid(3);
```

```
fprintf('Optimized PID Parameters: Kp=%.2f, Ki=%.2f, Kd=%.2f\n', Kp_opt, Ki_opt,
Kd_opt);

%% Run Simulation with Optimized PID Controller
tspan = [0 3600]; % 1-hour simulation
dt = 1;
t = 0:dt:tspan(2);
num_steps = length(t);
x = zeros(num_steps, length(x0));
x(1, :) = x0;
q_cw = zeros(num_steps, 1);
integral_error = 0;
prev_error = 0;

for i = 2:num_steps
    % Compute Error
    error = T_setpoint - x(i-1, 1);
    integral_error = integral_error + error * dt;
    derivative_error = (error - prev_error) / dt;

    % Compute PID Output
    q_cw(i) = Kp_opt * error + Ki_opt * integral_error + Kd_opt * derivative_error;
    q_cw(i) = max(0, min(q_cw(i), 8000));

    % Solve ODE
    [~, x_new] = ode15s(@(t, x) PID_Simple_Model_electrolyzer_model(t, x, par, Pnet,
q_cw(i)), [0 dt], x(i-1, :)');
    x(i, :) = x_new(end, :);
    prev_error = error;
end

%% Extract Results
T_el = x(:, 1:N); % Electrolyzer temperature
Psto_H2 = x(:, N+1); % H2 Storage pressure
Psto_O2 = x(:, N+2); % O2 Storage pressure
%% **Plot All Parameters After AI-Based PID Control**
%% **Plot All Parameters After AI-Based PID Control**
figure;

% **Electrolyzer Temperature**
subplot(4,2,1);
plot(t, T_el, 'LineWidth', 1.5);
hold on;
plot(xlim, [T_setpoint T_setpoint], '--r'); % horizontal line
text(mean(xlim), T_setpoint, 'Setpoint', 'VerticalAlignment', 'bottom',
'HorizontalAlignment', 'center');

xlabel('Time [s]');
ylabel('Electrolyzer Temperature [Â°C]');
title('Electrolyzer Temperature Control');
grid on;

% **Cooling Water Flow Rate**
subplot(4,2,2);
plot(t, q_cw, 'b', 'LineWidth', 1.5);
xlabel('Time [s]');
ylabel('Cooling Water Flow [g/s]');
title('PID-Controlled Cooling Water Flow');
grid on;

% **Hydrogen Storage Pressure**
subplot(4,2,3);
plot(t, Psto_H2, 'g', 'LineWidth', 1.5);
xlabel('Time [s]');
```

```
ylabel('H_2 Pressure [bar]');
title('Hydrogen Storage Pressure');
grid on;

% **Oxygen Storage Pressure**
subplot(4,2,4);
plot(t, Psto_O2, 'r', 'LineWidth', 1.5);
xlabel('Time [s]');
ylabel('O_2 Pressure [bar]');
title('Oxygen Storage Pressure');
grid on;

% **Buffer Tank Mass**
subplot(4,2,5);
plot(t, x(:, N+3), 'm', 'LineWidth', 1.5);
xlabel('Time [s]');
ylabel('Mass in Buffer Tank [g]');
title('Buffer Tank Mass Change');
grid on;

% **Buffer Tank Temperature**
subplot(4,2,6);
plot(t, x(:, N+4), 'k', 'LineWidth', 1.5);
xlabel('Time [s]');
ylabel('Buffer Tank Temp [Â°C]');
title('Buffer Tank Outlet Temperature');
grid on;

% **Electrolyzer Inlet Temperature**
subplot(4,2,7);
plot(t, x(:, N+5), 'c', 'LineWidth', 1.5);
xlabel('Time [s]');
ylabel('Electrolyzer Inlet Temp [Â°C]');
title('Electrolyzer Inlet Temperature');
grid on;

% **Net Power Input**
subplot(4,2,8);
plot(t, Pnet * ones(size(t)), 'y', 'LineWidth', 1.5);
xlabel('Time [s]');
ylabel('Power [W]');
title('Net Power Input');
grid on;

disp('âœ… All parameters plotted after AI-PID tuning.');

% **Electrolyzer Temperature**
figure;
plot(t, T_el, 'LineWidth', 1.5);
hold on;
yline(T_setpoint, '--r', 'Setpoint');
xlabel('Time [s]');
ylabel('Electrolyzer Temperature [Â°C]');
title('Electrolyzer Temperature Control');
grid on;

% **Cooling Water Flow Rate**
figure;
plot(t, q_cw, 'b', 'LineWidth', 1.5);
xlabel('Time [s]');
ylabel('Cooling Water Flow [g/s]');
title('PID-Controlled Cooling Water Flow');
grid on;
```

```
% **Hydrogen Storage Pressure**
figure;
plot(t, Psto_H2, 'g', 'LineWidth', 1.5);
xlabel('Time [s]');
ylabel('H_2 Pressure [bar]');
title('Hydrogen Storage Pressure');
grid on;

% **Oxygen Storage Pressure**
figure;
plot(t, Psto_O2, 'r', 'LineWidth', 1.5);
xlabel('Time [s]');
ylabel('O_2 Pressure [bar]');
title('Oxygen Storage Pressure');
grid on;

% **Buffer Tank Mass**
figure;
plot(t, x(:, N+3), 'm', 'LineWidth', 1.5);
xlabel('Time [s]');
ylabel('Mass in Buffer Tank [g]');
title('Buffer Tank Mass Change');
grid on;

% **Buffer Tank Temperature**
figure;
plot(t, x(:, N+4), 'k', 'LineWidth', 1.5);
xlabel('Time [s]');
ylabel('Buffer Tank Temp [Â°C]');
title('Buffer Tank Outlet Temperature');
grid on;

% **Electrolyzer Inlet Temperature**
figure;
plot(t, x(:, N+5), 'c', 'LineWidth', 1.5);
xlabel('Time [s]');
ylabel('Electrolyzer Inlet Temp [Â°C]');
title('Electrolyzer Inlet Temperature');
grid on;

% **Net Power Input**
figure;
plot(t, Pnet * ones(size(t)), 'y', 'LineWidth', 1.5);
xlabel('Time [s]');
ylabel('Power [W]');
title('Net Power Input');
grid on;

disp('âœ… All parameters plotted after AI-PID tuning.');
```

PID Simple Model parElectrolyzer :

```
function par = parElectrolyzer(N)

%Thisscriptdefinesvaluesoftheinputparametersforallelectrolyzers.
par.Const = ...
    struct('ze',2,'FC',96485,'R',8.314,'Cp',4.186,'CpLye',3.1006,...
    'Mwt',18,'MwtH2',2.01588,'Tref',25,'rho',1000,'rhoLye',1258.2,'Vc',...
    2.0681,'Vh',1.9944);

%Cp=specificheatofwater,[J/gK];Mwt=mol.wtofH2O,rho=densityof
%water/lye[kg/m3],Vc=volumeofcoldsideofheat...
%exchanger[m3],Vh=volumeof
```

```
%hotsideofheatexchanger[m3]

par.Comp = struct('alpha',0.63,'k',1.62,'Tel',25+273,'Pel',3);
par.Storage = struct('VstoH2',965000,'VstoO2',482500,'PoutH2',19,...
    'PoutO2',19,...
    'TstoH2',25+273.15,'TstoO2',25+273.15,'Rg',8.314e-2,'VdispH2',...
    0.5,'VdispO2',0.5);
%VstoH2andVstoO2areinlitres

par.Tw_in = 10;
%inlettemperatureofthecoolingwater inlyecirculationheatexchanger
par.Hex.UA = 20.48e3;
%UAofheatexchanger[W/K],basedonEoLdesign
par.kvalveH2 = 14.723;
%valveconstantfortheoutletvalveofhydrogenstoragetank,calculatedfor25barstoragepressure
atSS
par.kvalveO2 = 7.362;
%valveconstantfortheoutletvalveof
oxygenstoragetank,calculatedfor25barstoragepressureatSS
par.sigma = 5.672*10^-8;
%stefan-boltzmannconstant[W/mË†2KË†4]
par.em = 0.8;
%emissivity[-]
%ParametersforU-IrelationshipinUlleberg'smodel
par.U = struct([]);
par.TherMo = struct([]);
par.EL = struct([]);

for i =1:N
    %U-IcurveParameters
    par.U(i).r1 = 0.000218155; %ohmmË†2
    par.U(i).r2 = -0.000000425; %ohmmË†2CË†-1
    par.U(i).s = 0.1179375; %Vs
    par.U(i).t1 = -0.14529; %AË†-1mË†2
    par.U(i).t2 = 11.794; %AË†-1mË†2CË†-1
    par.U(i).t3 = 395.68; %AË†-1mË†2CË†-2
    par.U(i).f1 = 120; %mAË†2cmË†-4
    par.U(i).f2 = 0.98; %dimensionless
    %%Parametersforthethermalmodel
    par.TherMo(i).CtS = 625/27; %Specificthermalcapacity
ofelectrolyzeri.e.Ct/P,[kJ/kWatts*C]
    par.TherMo(i).Ct = 625/27*2135; %Cts*Pnom[kJ/C]or[kJ/K],AssumingPnom=2135kWatts
    par.TherMo(i).hc = 5.5; %convectiveheattransfer coefficientW/mË†2C
    par.TherMo(i).A_surf = 0.1; %specificraditionareaper
kAcurrentpercell,[mË†2/kA*Ncell]
    par.TherMo(i).A_El = 0.1*5.72*230; %surfaceareaofthe
electrolyzer,A_surf*Inom*Ncell[mË†2]
    %%ParametersforFaradayeffeciencycalculations
    par.EL(i).Utn = 1.482; %thermoneutralvoltage,[V]
    par.EL(i).nc = 230; %no.ofcells
    par.EL(i).A = 2.6; %electrodeareaofeach cell,[mË†2]
    par.EL(i).Ta = 20; %ambienttemp,[C]
    par.EL(i).Tstd = 25; %standardtemperature,[C]
end

%El#2,performingat85%ofelectrolyzer1
par.U(2).r1 = par.U(2).r1*1.2; %ohmmË†2
par.U(2).s = par.U(2).s*1.2; %V
par.U(2).f1 = par.U(2).f1*1.2; %mAË†2cmË†-4
par.U(2).f2 = 0.97; %El#3,performingat70%ofelectrolyzer1
par.U(3).r1 = par.U(3).r1*1.3; %ohmmË†2
par.U(3).s = par.U(3).s*1.3; %V
par.U(3).f1 = par.U(3).f1*1.3; %mAË†2cmË†-4
par.U(3).f2 = 0.96;
par.N=N;
```

```
end
```

3. MPC Model :

MPC Simple Model:

```
clc;
clear;
close all;

%% Load Electrolyzer Parameters
N = 3; % Number of electrolyzers
par = MPC_Simple_Model_parElectrolyzer(N);

%% Define Simulation Time
num_hr = 0.25; % Simulation duration in hours
tspan = [0 num_hr * 3600]; % Convert hours to seconds

%% Initial Conditions
Pnet = 9e6; % Total input power [W]
x0 = [75*ones(N,1);  % Electrolyzer temperature [Â°C]
      25;            % H2 Storage pressure [bar]
      25;            % O2 Storage pressure [bar]
      6000000;       % Buffer tank mass [g]
      70;            % Buffer tank outlet temp [Â°C]
      65;            % Electrolyzer inlet temp [Â°C]
      20];           % Cooling water outlet temp [Â°C]

%% Define State-Space Model for MPC
A = -0.02; % Approximate system dynamics
B = 0.01;  % Control input effect
C = 1;     % Output mapping (temperature)
D = 0;

sys = ss(A, B, C, D); % Create state-space model

%% Configure MPC Controller
mpcController = mpc(sys, 1); % Sampling time = 1 sec
mpcController.PredictionHorizon = 10;
mpcController.ControlHorizon = 2;

% Define Constraints
mpcController.MV(1).Min = 0;      % Min cooling water flow rate
mpcController.MV(1).Max = 80000;  % Max cooling water flow rate
mpcController.OV(1).Min = 60;     % Min electrolyzer temp
mpcController.OV(1).Max = 80;     % Max electrolyzer temp

% Set Optimization Weights
mpcController.Weights.ManipulatedVariables = 0.1;
mpcController.Weights.ManipulatedVariablesRate = 0.01;
mpcController.Weights.OutputVariables = 1;

%% **Initialize MPC State**
mpcState = mpcstate(mpcController);

%% Run Simulation with MPC
T_setpoint = 75; % Desired electrolyzer temperature
q_cw = zeros(length(tspan), 1); % Cooling water flow rate

[t, x] = ode15s(@(t, x) MPC_Simple_Model_electrolyzer_model(t, x, par, Pnet, q_cw(1)),
tspan, x0);
```

```
for i = 2:length(t)
    % Compute MPC-based cooling water flow using the correct state object
    q_cw(i) = mpcmove(mpcController, mpcState, x(i-1,1), T_setpoint);

    % Simulate the system for the next step
    [~, x_next] = ode15s(@(t, x) MPC_Simple_Model_electrolyzer_model(t, x, par, Pnet,
q_cw(i)), [t(i-1) t(i)], x(i-1, :));
    x(i, :) = x_next(end, :);
end

%% Extract Results
T_el = x(:, 1:N); % Electrolyzer temperature
Psto_H2 = x(:, N+1); % H2 Storage pressure
Psto_O2 = x(:, N+2); % O2 Storage pressure
T_bt_out = x(:, N+4); % Buffer tank outlet temperature

%% **Plot Results**
%% Plot results with setpoint line
figure;
plot(t, x(:,1), 'b', 'LineWidth', 2); % Electrolyzer temperature
hold on;
plot([t(1), t(end)], [T_setpoint, T_setpoint], '--r', 'DisplayName', 'Setpoint'); %
Setpoint line
xlabel('Time [s]');
ylabel('Electrolyzer Temperature [°C]');
title('Electrolyzer Temperature vs Time');
legend('Temperature', 'Setpoint');
grid on;

figure;
plot(t, q_cw, 'b', 'LineWidth', 1.5);
xlabel('Time [s]');
ylabel('Cooling Water Flow Rate [g/s]');
title('MPC-Controlled Cooling Water Flow');
grid on;

figure;
plot(t, Psto_H2, 'g', 'LineWidth', 1.5);
xlabel('Time [s]');
ylabel('H_2 Storage Pressure [bar]');
title('Hydrogen Storage Pressure');
grid on;

figure;
plot(t, Psto_O2, 'r', 'LineWidth', 1.5);
xlabel('Time [s]');
ylabel('O_2 Storage Pressure [bar]');
title('Oxygen Storage Pressure');
grid on;

disp('âœ… Simulation completed successfully.');
```

MPC Simple Model electrolyzer model:

```
function dxdt = Simple_Model_electrolyzer_model(t, x, par, Pnet, q_cw)
% ELECTROLYZER_MODEL - Differential equations for the electrolyzer system
% INPUTS:
%   t    - Time (unused, required for ode solver)
%   x    - State vector [Temperatures, Pressures, Mass]
%   par  - Electrolyzer parameters (struct)
%   Pnet - Total input power [W]
%   q_cw - Cooling water flow rate [g/s]
% OUTPUT:
```

```
%   dxdt - Time derivatives of the state variables

N = par.N; % Number of electrolyzers

% Extract states
T_el = x(1:N);       % Electrolyzer temperatures [Â°C]
Psto_H2 = x(N+1);    % Hydrogen storage pressure [bar]
Psto_O2 = x(N+2);    % Oxygen storage pressure [bar]
Mass_Bt = x(N+3);    % Buffer tank mass [kg]
T_bt_out = x(N+4);   % Buffer tank outlet temperature [Â°C]
T_El_in = x(N+5);    % Electrolyzer inlet temperature [Â°C]

% Electrochemical equations
F_const = 96485;       % Faraday constant [C/mol]
Utn = 1.482;          % Thermoneutral voltage [V]
I_el = Pnet / (Utn * par.EL(1).nc); % Estimated current
H2_production = I_el * par.EL(1).nc / (2 * F_const); % Hydrogen flow [mol/s]

% Energy balance
Q_generated = (Pnet - H2_production * Utn * F_const);
Q_loss = 5.5 * (T_el - 25) + 5.67e-8 * 0.8 * ((T_el.^4) - (25^4));
Q_net = Q_generated - Q_loss - q_cw .* (T_el - T_El_in);

% Mass balance
Water_consumption = H2_production * 18; % Water loss [g/s]

% Differential equations
dxdt = zeros(N+6, 1);
dxdt(1:N) = (Q_net) ./ (par.EL(1).A * par.EL(1).nc); % Temperature dynamics
dxdt(N+1) = H2_production - Psto_H2 / 100;  % Hydrogen storage pressure
dxdt(N+2) = 0.5 * H2_production - Psto_O2 / 100;  % Oxygen storage pressure
dxdt(N+3) = -Water_consumption;  % Buffer tank mass change
dxdt(N+4) = (T_El_in - T_bt_out) / 10;  % Buffer tank outlet temperature
dxdt(N+5) = (q_cw - T_El_in) / 10;  % Electrolyzer inlet temperature
dxdt(N+6) = 0;  % Cooling water outlet (constant for now)

end
```

MPC Simple Model parElectrolyzer:

```
function par = parElectrolyzer(N)

%Thisscriptdefinesvaluesoftheinputparametersforallelectrolyzers.
par.Const = ...
    struct('ze',2,'FC',96485,'R',8.314,'Cp',4.186,'CpLye',3.1006,...
    'Mwt',18,'MwtH2',2.01588,'Tref',25,'rho',1000,'rhoLye',1258.2,'Vc',...
    2.0681,'Vh',1.9944);

%Cp=specificheatofwater,[J/gK];Mwt=mol.wtofH2O,rho=densityof
%water/lye[kg/m3],Vc=volumeofcoldsideofheat...
%exchanger[m3],Vh=volumeof
%hotsideofheatexchanger[m3]

par.Comp = struct('alpha',0.63,'k',1.62,'Tel',25+273,'Pel',3);
par.Storage = struct('VstoH2',965000,'VstoO2',482500,'PoutH2',19,...
    'PoutO2',19,...
    'TstoH2',25+273.15,'TstoO2',25+273.15,'Rg',8.314e-2,'VdispH2',...
    0.5,'VdispO2',0.5);
%VstoH2andVstoO2areinlitres

par.Tw_in = 10;
%inlettemperatureofthecoolingwater inlyecirculationheatexchanger
par.Hex.UA = 20.48e3;
```

```
%UAofheatexchanger[W/K],basedonEoLdesign
par.kvalveH2 = 14.723;
%valveconstantfortheoutletvalveofhydrogenstoragetank,calculatedfor25barstoragepressure
atSS
par.kvalveO2 = 7.362;
%valveconstantfortheoutletvalveof
oxygenstoragetank,calculatedfor25barstoragepressureatSS
par.sigma = 5.672*10^-8;
%stefan-boltzmannconstant[W/mË†2KË†4]
par.em = 0.8;
%emissivity[-]
%ParametersforU-IrelationshipinUlleberg'smodel
par.U = struct([]);
par.TherMo = struct([]);
par.EL = struct([]);

for i =1:N
    %U-IcurveParameters
    par.U(i).r1 = 0.000218155; %ohmmË†2
    par.U(i).r2 = -0.000000425; %ohmmË†2CË†-1
    par.U(i).s = 0.1179375; %Vs
    par.U(i).t1 = -0.14529; %AË†-1mË†2
    par.U(i).t2 = 11.794; %AË†-1mË†2CË†-1
    par.U(i).t3 = 395.68; %AË†-1mË†2CË†-2
    par.U(i).f1 = 120; %mAË†2cmË†-4
    par.U(i).f2 = 0.98; %dimensionless
    %%Parametersforthethermalmodel
    par.TherMo(i).CtS = 625/27; %Specificthermalcapacity
ofelectrolyzeri.e.Ct/P,[kJ/kWatts*C]
    par.TherMo(i).Ct = 625/27*2135; %Cts*Pnom[kJ/C]or[kJ/K],AssumingPnom=2135kWatts
    par.TherMo(i).hc = 5.5; %convectiveheattransfer coefficientW/mË†2C
    par.TherMo(i).A_surf = 0.1; %specificraditionareaper
kAcurrentpercell,[mË†2/kA*Ncell]
    par.TherMo(i).A_El = 0.1*5.72*230; %surfaceareaofthe
electrolyzer,A_surf*Inom*Ncell[mË†2]
    %%ParametersforFaradayeffeciencycalculations
    par.EL(i).Utn = 1.482; %thermoneutralvoltage,[V]
    par.EL(i).nc = 230; %no.ofcells
    par.EL(i).A = 2.6; %electrodeareaofeach cell,[mË†2]
    par.EL(i).Ta = 20; %ambienttemp,[C]
    par.EL(i).Tstd = 25; %standardtemperature,[C]
end

%El#2,performingat85%ofelectrolyzer1
par.U(2).r1 = par.U(2).r1*1.2; %ohmmË†2
par.U(2).s = par.U(2).s*1.2; %V
par.U(2).f1 = par.U(2).f1*1.2; %mAË†2cmË†-4
par.U(2).f2 = 0.97; %El#3,performingat70%ofelectrolyzer1
par.U(3).r1 = par.U(3).r1*1.3; %ohmmË†2
par.U(3).s = par.U(3).s*1.3; %V
par.U(3).f1 = par.U(3).f1*1.3; %mAË†2cmË†-4
par.U(3).f2 = 0.96;
par.N=N;
end
```